NAVAL POSTGRADUATE SCHOOL

MONTEREY, CALIFORNIA

THESIS

AUTOMATING IDENTIFICATION OF ROADS AND TRAILS UNDER CANOPY USING LIDAR

by

Charles F. Harmon III

September 2011

Thesis Advisor:	Richard C. Olsen
Second Reader:	Kristen Tsolis

Approved for public release; distribution is unlimited

THIS PAGE INTENTIONALLY LEFT BLANK

REPORT DOCUMENTATION PAGE			Form Approved OMB No. 0704–0188
Public reporting burden for this collection of information is estimated to average 1 hour per response, including the time for reviewing instruction, searching existing data sources, gathering and maintaining the data needed, and completing and reviewing the collection of information. Send comments regarding this burden estimate or any other aspect of this collection of information, including suggestions for reducing this burden, to Washington headquarters Services, Directorate for Information Operations and Reports, 1215 Jefferson Davis Highway, Suite 1204, Arlington, VA 22202–4302, and to the Office of Management and Budget, Paperwork Reduction Project (0704–0188) Washington DC 20503.			
1. AGENCY USE ONLY *(Leave blank)*	**2. REPORT DATE** September 2011	**3. REPORT TYPE AND DATES COVERED** Master's Thesis	
4. TITLE AND SUBTITLE Automating Identification of Roads and Trails Under Canopy Using LIDAR		**5. FUNDING NUMBERS**	
6. AUTHOR Charles F. Harmon III			
7. PERFORMING ORGANIZATION NAME(S) AND ADDRESS(ES) Naval Postgraduate School Monterey, CA 93943–5000		**8. PERFORMING ORGANIZATION REPORT NUMBER**	
9. SPONSORING /MONITORING AGENCY NAME(S) AND ADDRESS(ES) N/A		**10. SPONSORING/MONITORING AGENCY REPORT NUMBER**	
11. SUPPLEMENTARY NOTES The views expressed in this thesis are those of the author and do not reflect the official policy or position of the Department of Defense or the U.S. Government. IRB Protocol number NA.			
12a. DISTRIBUTION / AVAILABILITY STATEMENT Approved for public release; distribution is unlimited		**12b. DISTRIBUTION CODE**	

13. ABSTRACT (maximum 200 words)

Analysis techniques are developed to automatically extract roads and trails under thick forest canopy. LiDAR data were taken over the Swanton Pacific Ranch in the Santa Cruz Mountains from an airborne laser mapping system, the Optech 3100, on March 9–10, 2010. Collected data were characterized by point densities of 5–10 m^2. Point cloud data were reduced to digital surface models using ARCMAP (from ESRI). The DSM was calculated at 1 meter spacing. These surface models were analyzed using topographic tools in ENVI, allowing for calculation of curvature, slope, convexity, and shaded relief. A multi-layer dataset was built and analyzed using spectral analysis tools in ENVI. The classification technique used was a combination of maximum likelihood classifier and a decision tree after use of erosion/dilation operators. Results are compared to ground truth collected in 2011. Classification resulted in 83.6% true positive rate, and the image processing result reduced the false positive rate to 3.0%.

14. SUBJECT TERMS LiDAR, LADAR, Swanton Pacific Ranch, Feature Extraction			**15. NUMBER OF PAGES** 91
			16. PRICE CODE
17. SECURITY CLASSIFICATION OF REPORT Unclassified	**18. SECURITY CLASSIFICATION OF THIS PAGE** Unclassified	**19. SECURITY CLASSIFICATION OF ABSTRACT** Unclassified	**20. LIMITATION OF ABSTRACT** UU

NSN 7540–01–280–5500 Standard Form 298 (Rev. 2–89)
Prescribed by ANSI Std. 239–18

THIS PAGE INTENTIONALLY LEFT BLANK

Approved for public release, distribution is unlimited

AUTOMATING IDENTIFICATION OF ROADS AND TRAILS UNDER CANOPY USING LIDAR

Charles F. Harmon III
Major, United States Army
B.A., University of North Carolina – Chapel Hill, 1999

Submitted in partial fulfillment of the
requirements for the degree of

MASTER OF SCIENCE IN SPACE SYSTEMS OPERATIONS
and
MASTER OF SCIENCE IN REMOTE SENSING INTELLIGENCE

from the

NAVAL POSTGRADUATE SCHOOL
September 2011

Author: Charles F. Harmon III

Approved by: Richard C. Olsen
Thesis Advisor

Kristen Tsolis
Second Reader

Dan C. Boger
Chair, Department of Information Science

Rudy Panholzer
Chair, Department of Space Systems Academic Group

THIS PAGE INTENTIONALLY LEFT BLANK

ABSTRACT

Analysis techniques are developed to automatically extract roads and trails under thick forest canopy. LiDAR data were taken over the Swanton Pacific Ranch in the Santa Cruz Mountains from an airborne laser mapping system, the Optech 3100, on March 9–10, 2010. Collected data were characterized by point densities of 5–10 m^2. Point cloud data were reduced to digital surface models using ARCMAP (from ESRI). The DSM was calculated at 1 meter spacing. These surface models were analyzed using topographic tools in ENVI, allowing for calculation of curvature, slope, convexity, and shaded relief. A multi-layer dataset was built and analyzed using spectral analysis tools in ENVI. The classification technique used was a combination of maximum likelihood classifier and a decision tree after use of erosion/dilation operators. Results are compared to ground truth collected in 2011. Classification resulted in 83.6% true positive rate, and the image processing result reduced the false positive rate to 3.4%.

THIS PAGE INTENTIONALLY LEFT BLANK

TABLE OF CONTENTS

THIS PAGE INTENTIONALLY LEFT BLANK

LIST OF FIGURES

LIST OF TABLES

THIS PAGE INTENTIONALLY LEFT BLANK

LIST OF ACRONYMS AND ABBREVIATIONS

AGL	Above Ground Level
ALPS	Airborne Laser Profiling System
ALTM	Airborne Laser Terrain Mapper
ASPRS	American Society for Photogrammetry and Remote Sensing
Cal Poly	California Polytechnic State University
CW	Continuous Wave
DEM	Digital Elevation Model
DSM	Digital Surface Model
DTM	Digital Terrain Model
ENVI	Environment for Visualizing Images
ESRI	Economic and Social Research Institute
GLAS	Geoscience Laser Altimeter System
GPS	Global Positioning System
ICESat	Ice, Cloud, and Land Elevation Satellite
IMU	Inertial Measuring Unit
IPB	Intelligence Preparation of the Battlefield
LiDAR	Light Detection And Ranging
LITE	LiDAR In Space Technology Experiment
LOC	Lines Of Communications
MPIA	Multiple Pulses In Air
NASA	National Aeronautics and Space Administration
nDSM	Normalized Digital Surface Model
NPS	Naval Postgraduate School
PCD	Phase Coded Disk
PRF	Pulse Repetition Frequency
RaDAR	Radio Detection And Ranging
ROI	Region Of Interest
SLA	Shuttle Laser Altimeter
STS	Space Transportation System
TIN	Triangulated Irregular Network

TOF	Time Of Flight
UTM	Universal Transverse Mercator

ACKNOWLEDGMENTS

I would like to extend special thanks to my advisor, Dr. R. C. Olsen, and second reader, Ms. Kristen Tsolis, for your support and guidance throughout this research. To the faculty and staff of the Remote Sensing Center at the Naval Postgraduate School, particularly Dr. Fred Kruse, Ms. Angie Kim, and Ms. Krista Lee, your knowledge, direction, and enthusiasm made coming to work every day a joy.

To my friends and colleagues here at the Naval Postgraduate School, LCDR Kenny Myrick, Major Josh Nagtzaam, Captain Cory Scott, and Captain Steve Muha, thanks for motivating me to finish this. You all have helped pull me to the end of this journey.

Last, but certainly not least, thanks go to my wonderful family: son, Aidan, and wife, Cariann Colman. Without your support and love none of this would have been possible.

THIS PAGE INTENTIONALLY LEFT BLANK

I. INTRODUCTION

A. PURPOSE OF RESEARCH

During intelligence preparation of the battlefield (IPB), intelligence analysts must describe the operational environment for the commander. This includes mapping the lines of communications (LOC) that traverse the area of operations. Traditional methods of remote sensing cannot identify roads and trails beneath dense canopy. LiDAR (Light Detection and Ranging) is a remote sensing technology used to create digital elevation models (DEM) of the Earth's surface, and has the capability to penetrate forest canopy to identify roads and trails beneath. This research will use classification methods and image processing techniques to automatically identify trails beneath dense forest canopy, to provide a tool for intelligence analysts in support of ground maneuver forces.

LiDAR, like RADAR, is an acronym which stands for light detection and ranging, and also describes the process by which LiDAR systems create 3D point cloud models of terrain and above ground objects (Gordon & Charles, 2008). LiDAR systems measure the time-of-flight for a laser pulse to travel from a sensor to a reflective object and back. Over the last decade, topographic laser profiling and scanning (LiDAR) systems have made major improvements in accuracy and application. Installed on airborne, spaceborne, or terrestrial-based platforms these sensors are approaching horizontal and vertical accuracies on the order of centimeters (Vosselman & Maas, 2010). These sensors fire a beam of light that travels toward the target, i.e., ground. If the beam strikes anything on its way to the ground, such as a tree, part of the beam's energy is reflected back to the sensor and recorded as the first return. The rest of the beam continues to the ground or some other solid surface that prevents further progress and reflects back to the sensor as the last return (Crutchley & Crow, 2009). Early systems generally only recorded the first and last returns since these measurements were used to create the digital surface models (DSM) and digital terrain model (DTM) respectively. Modern systems record up to an industry standard four returns, and a few systems are capable of providing full waveform data as described in Figure 1.

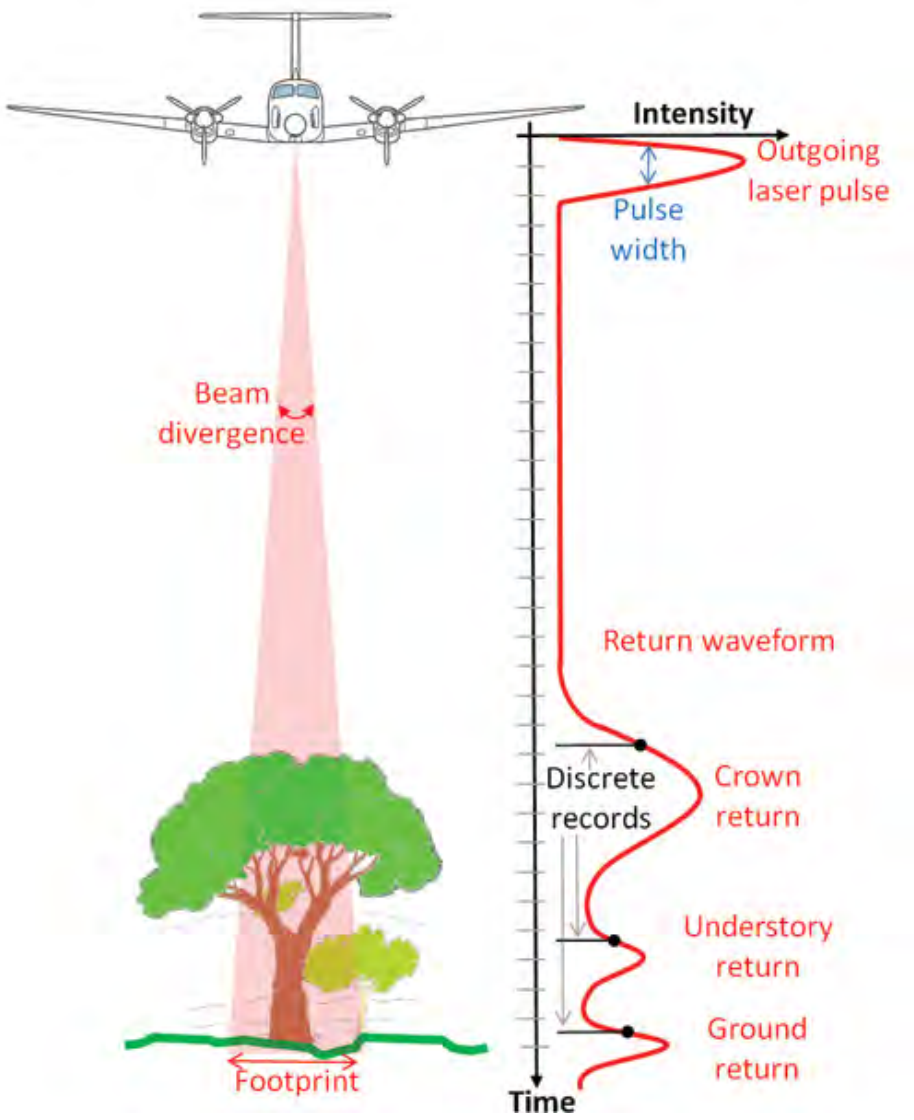

Figure 1. Full waveform LiDAR versus discrete recording characteristics (From Diaz, 2011)

Of the total land mass of Earth, forests cover 31%; this was estimated to be over 10 billion acres in 2010 (Food and Agriculture Organization of the United Nations, 2010). Traditional imaging systems are unable to observe beneath these forest canopies, allowing freedom of maneuver for illicit organizations and terrorist activities. As discussed earlier, LiDAR can penetrate forest canopies and identify the surface characteristics and any manmade structures under cover of trees. Previous work on this subject has proven the feasibility of using LiDAR to identify roads and trails beneath

dense canopy (Espinoza & Owens, 2007). The purpose of this research is to develop an automated process to identify roads and trails under tree cover from large LiDAR data sets.

B. OBJECTIVE

The primary objective of this thesis is to detect roads and trails in a forested region of Santa Cruz County, CA, from airborne LiDAR data. The LiDAR data set was collected in 2010 for California Polytechnic State University (Cal Poly) for their Swanton Pacific Ranch study area. Using products derived from the LiDAR point cloud, roads and trails are characterized and classified using a decision tree approach, where the union of a maximum likelihood classification and a Laplacian edge enhancement produces the final product.

A brief history of the development of LiDAR is presented in the background section as well as a discussion of the different terrestrial, airborne, and spaceborne applications of LiDAR. A short explanation of laser fundamentals and laser ranging is included to illustrate the basic measurement principles of LiDAR systems. The problem and observations sections describe the areas of study, the equipment and software used, and the experimental setup. The analysis and summary sections provide conclusions drawn from the research and experimental results.

THIS PAGE INTENTIONALLY LEFT BLANK

II. BACKGROUND

A. BACKGROUND

1. Brief History of LiDAR Development

RADAR (Radio Detection And Ranging) is the process of transmitting, receiving, detecting, and processing electromagnetic waves, and was invented by the German Army in 1935 (Richmond & Cain, 2010). Since then, this process has expanded to use in other areas of the magnetic spectrum from centimeter waves, to millimeter and microwave ranges, and with the advent of lasers to optical wavelengths.

In 1960, the invention of the ruby laser was followed by a decade of rapid development for laser technology. Shortly after, laser surveying instruments were proven in experimental use with the first laser altimeters flown from aircraft as early as 1965 in the United Kingdom by Shepherd. Later that same year, Miller, Jensen and Ruddock introduced the first airborne laser profiler for commercial topographic mapping by a joint venture of Spectra Physics Company (built the laser) and Aero Service Corporation (aerial survey and mapping company) (Gordon & Charles, 2008). During the 1970s and 1980s, laser profiling systems experienced steady development, typically using Nd:YAG solid state lasers or GaAs semiconductor lasers. The systems developed during this time used two-axis gyros to measure the aircraft attitude and used microwave transponders that calculated aircraft position and altitude based on triangulation from three surveyed ground stations.

It was not until the advent of global positioning system (GPS), inertial measuring units (IMU) for aircraft, and improved computer processing in the 1990s that laser scanners could achieve the accuracies needed to make them commercially viable for topographic mapping (Heritage & Large, 2009). In 1989, Dr. Joachim Lindenberger conducted extensive testing of an airborne laser profiling system (ALPS) that used a Sercel GPS receiver in conjunction with a Delco Carrousel IMU for position and attitude determination. Optech added a scanning mechanism to the system three years later. The

resulting Airborne Laser Terrain Mapper (ALTM) 1020 was the first LiDAR system that had all of the components of modern systems (Gordon & Charles, 2008).

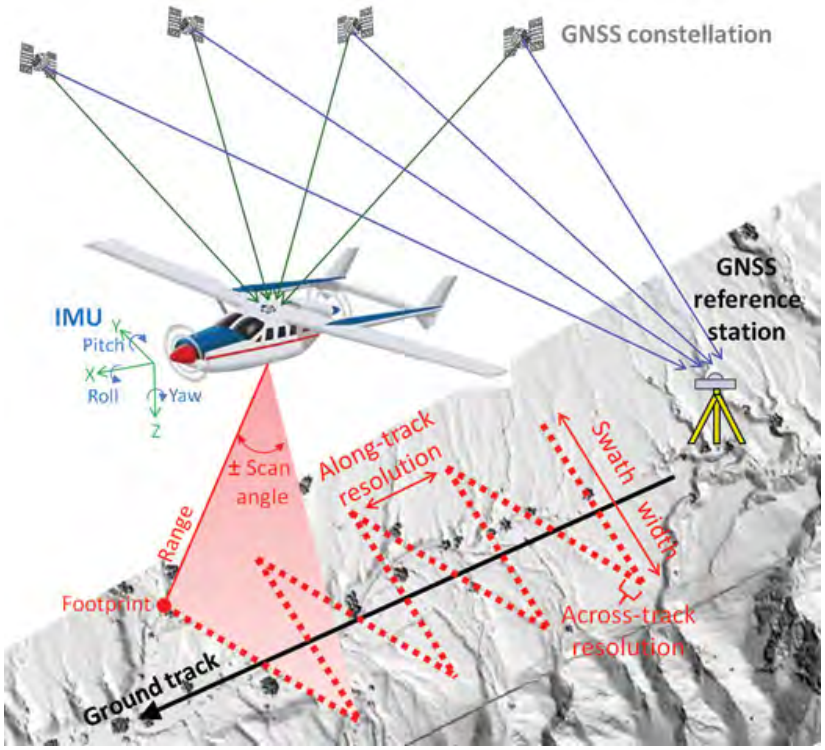

Figure 2. Basic operating principles of airborne mapping LiDAR with enabling technologies: Global Navigation Satellite System (GNSS), IMU, and laser scanner (From Diaz, 2011)

2. Laser Fundamentals

Within the context of LiDAR, any point on the Earth's surface can be described by its x, y, and z coordinates. A LiDAR system can construct these points from three sources: the LiDAR sensor, the IMU of the aircraft, and the GPS (Heritage & Large, 2009). A scanning LiDAR system corrects measurements for the yaw, pitch, and roll of the aircraft and the side-to-side scanning mechanism of the LiDAR sensor. The GPS units allow the measurements to be overlaid relative to the WGS84 datum. The following discussion describes lasers in general and laser ranging in detail.

LiDAR shares many of the same characteristics as radar, such as waveform and propagation time, albeit at a different frequency band. Where radars operate over a wide

range of frequencies, usually based on target characteristics and atmospheric attenuation, lasers are limited to discrete laser lines and usually operate in the near infrared based on acceptable lasers and detectors (Richmond & Cain, 2010). LiDAR systems' pulse repetition frequency (PRF) greatly affects resolution; as systems with higher PRFs can measure more points in a given area of study.

Generally, lasers are classified by the material used as a radiation source, most commonly gas lasers, solid-state lasers, and semi-conductor lasers. Lasers used for topographic mapping are required to have high intensity and have a high degree of collimation, that is the light rays are near parallel, and will spread slowly as it propagates (Gordon & Charles, 2008). Given these requirements, the most common laser types used for topographic mapping are solid-state lasers using neodymium-doped yttrium aluminum garnet (Nd:YAG) and semiconductor lasers using gallium arsenide (GaAs). These materials when coupled with an energy source and two mirrors, one fully reflective, and the other semi reflective make up the components of every laser.

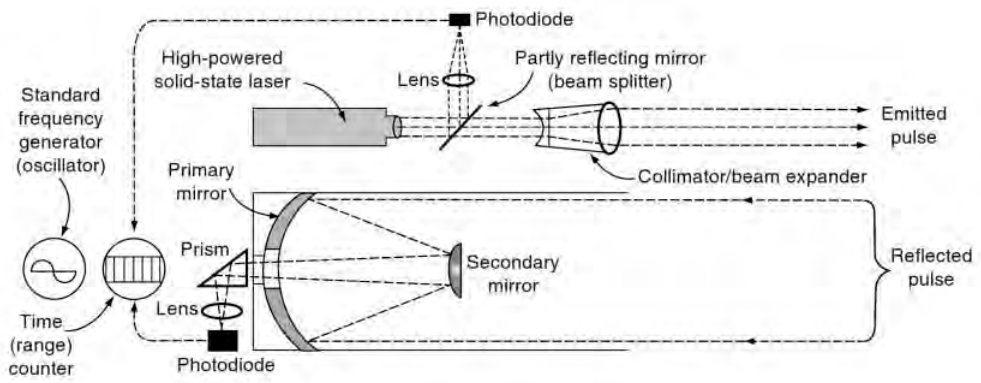

Figure 3. Layout of the main components of a pulse-type laser rangefinder (From Shan & Toth, 2009)

Once one has the components that make up a laser, all ranging, profiling, and scanning are based on laser ranging instrument that can measure distance to a very high degree of accuracy. There are two main methods of measuring range using laser: the time of flight (TOF) method and the phase comparison method. The TOF method very accurately measures how long it takes a laser pulse to travel from the emitter to the target

and back to a receiver. The phase comparison method measures the phase difference in the sinusoidal pattern emitted by a continuous wave (CW) laser. Due to the limited power of CW lasers there are very few phase comparison systems used in airborne or spaceborne topographic mapping (an exception is the ScaLARS research laser scanner) and will not be discussed further (Shan & Toth, 2009).

The TOF method for LiDAR is analogous to range equations for radar systems the measure the precise travel time for an emitted pulse. The relationship between the range to the target and the time for the pulse to make the round way trip to the target and back to the receiver is:

$$R=\frac{c\tau}{2}$$

Where R is the slant range to the target, c is the speed of light, which is known, and τ is the measured time interval. Since the speed of light is very accurately known, the accuracy of the range measurement depends largely on the precision of the time measurement and the method of defining the leading edge of the returning pulse (no rectangular pulses) (Baltsavias, 1999). For example, to achieve a 1 cm resolution the timer should be able to measure a 66ps interval which requires a clock rate of approximately 15GHz (Shan & Toth, 2009).

As with RADAR, technology approaches have devised to make longer pulses more practical. The range equation is a tool that is widely used in the literature that relates the power received (P_r) after being reflected from a target from a laser pulse with a given power transmitted (P_t). Baltsavias (1999) provides an explanation of the following equation:

$$P_r = \rho \frac{\eta^2 A_r}{\pi R^2} P_T$$

Where ρ is the reflectivity of the target, η is atmospheric transmission, A_r is the area of the receiving optics, and R is the range form the LiDAR sensor to the target. This equation assumes the laser footprint and detector (optics) completely covers the target area and the reflected power radiates uniformly in a hemisphere. This simplified

equation is an optimistic approximation since several other factors internal to specific LiDAR systems introduce additional losses, but the equation does show that at increased sensor heights (greater range) P_T and A_r must be increased to get useful signal.

As an example, the Optech 3100 system that collected the data for this study has a peak transmission power, P_T = 980 watts and a standard operating range of 3,000 ft, and receiver area of 10cm^2 (Optech, 2011). Assuming a typical mid-latitude transmittance of 0.6 and reflectivity of 0.5, both for wavelength 1064 nm the above equation yields:

$$P_r = 0.5\frac{(0.6)^2(0.01m^2)}{\pi(914m)^2}980\text{W}$$

$$P_r = 6.72\times10^{-7}\text{ W}$$

Depending on the distances being measured, it is possible to make a large number of measurements over a short period of time. This is known as the pulse repetition frequency and for most commercial systems typically ranges from 33 to 167 kHz. To continue with the Optech 3100 example: if a distance of 3,000 ft (914 m) needs to be measured, then the travel time over the 6,000 ft out and back of the pulse is:

$$T=\frac{2*R}{c}$$

$$T=\frac{2*(914\text{m})}{2.998\times10^8\frac{\text{m}}{\text{s}}}=6.1\times10^{-6}s$$

$$PRF=\frac{1}{6.1\times10^{-6}s}=164\text{kHz}$$

Thus the maximum PRF of the system operating at 3,000 ft is 164 kHz, and generally the higher the operating altitude the longer time interval required between successive pulses (Shan & Toth, 2009). However, multiple pulse techniques are starting to be introduced which allows for more than one pulse to be in the air at a time, known as multiple pulses in air (MPIA). These systems' PRF are no longer limited by altitude and pulse time-of-flight, but only limited by how frequently a pulse can be emitted from the laser source. As a practical example, the Optech Pegasus advertises a PRF of 500 kHz at an operating altitude of 300 m or 225 kHz at 1,000 m altitude (Optech, 2011).

3. Applications of LiDAR

LiDAR systems are generally used in one of three distinct realms based on the platform of the laser scanner: terrestrial, airborne, and spaceborne. Each type of application has distinct processes, and based on system advantages and disadvantages are used by different scientific and surveying communities.

Since the beginning of laser range finders, surveyors have used light ranging systems for distance and range measurements (Shan & Toth, 2009). In the community of field surveying, lasers began to replace tungsten and mercury vapor lamps in electronic distance measuring instrument in the 1970s. These instruments were only used initially for measuring distances for control surveys or geodetic networks, but theodolites were used separately to measure the angles needed for these operations. Eventually, these separate systems were consolidated, and with the advent of small eye-safe lasers, reflectorless distance measurements became possible (Gordon & Charles, 2008). This evolution in the different field surveying applications, led to the current tripod and vehicle-mounted laser scanning systems being used for topographic mapping applications, such as Google Maps Street View, which uses three lasers to capture 3D data (Google).

For spaceborne LiDAR systems, the challenging operational environment has made development slow. Spaceborne LiDAR systems function under the same principles described earlier, however, with distances and speeds 100 times greater than that of an airborne LiDAR system. Much more powerful lasers are required and system PRFs are much reduced. For these reasons, spaceborne LiDAR systems to date have been laser profiling systems and not laser scanning systems, only measuring pulses along track of the spacecraft with no side-to-side swath measurements. Due to pressures from various scientific communities that were concerned with accurate elevation data for ice-covered terrain and desert regions, NASA began several Space Shuttle experiments beginning with the mission, LITE (LiDAR In-space Technology Experiment) (NASA, 1994). Conducted in 1994, onboard STS-64, the LITE payload was a 2 metric ton system that operated on three different wavelengths: 1064 nm, 532 nm, and 355 nm and was principally concerned with atmospheric, climatic, and weather research. The success of

LITE led to two additional shuttle experiments in 1996 and 1997, named Shuttle Laser Altimeter (SLA). The first mission, SLA-01, was on STS-72 and operated for over 80 hours measuring over 475,000 pulses returned from land surfaces. The tracks for SLA-01 are in Figure 4.

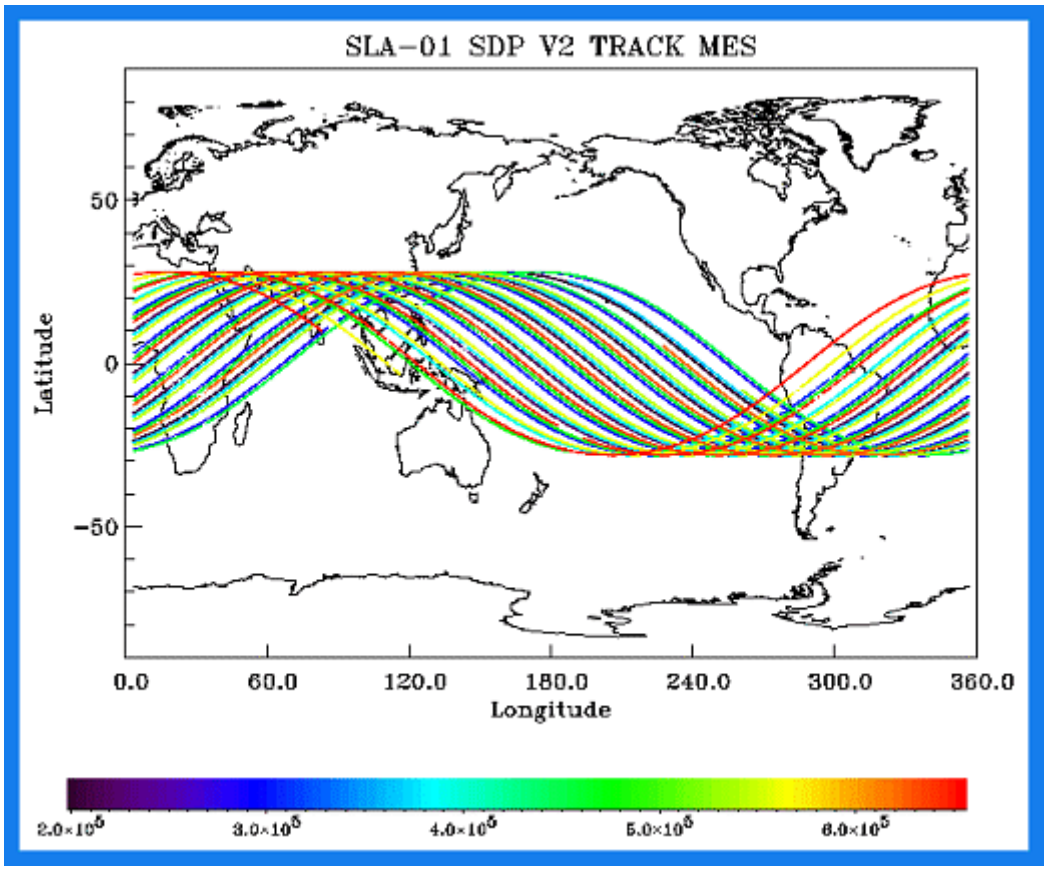

Figure 4. Ground track of STS-72 while collecting data for SLA-01. Color ramp indicates altitude in meters (From Harding, 2001)

The second experiment took place on STS-85 in August, 1997. SLA-02 generated 100 m laser footprints on the ground at a PRF of 10 Hz and wavelength of 1064nm giving a ground spot spacing of 700 m (Carabajal et al., 1999). These experiments were the precursors to the Geoscience Laser Altimeter System (GLAS) that is the primary payload on the Ice, Cloud, and land Elevation Satellite (ICESat). Launched in January 2003, GLAS has the primary mission of monitoring the Earth's ice sheets to determine changes in total mass and any contribution to sea level changes

(Schutz, Zwally, Shuman, Hancock, & DiMarzio, 2005). GLAS operates at two wavelengths, 1064 nm and 532 nm, and from an altitude of 600 km creates a 70 m laser spot along the ground track at 40 Hz PRF resulting in 170 m interval pulses (Abshire et al., 2005). ICESat was decommissioned on August 17, 2010, after a successful seven years of operations. Figure 5 describes tree canopy height in the United States from data collected by GLAS.

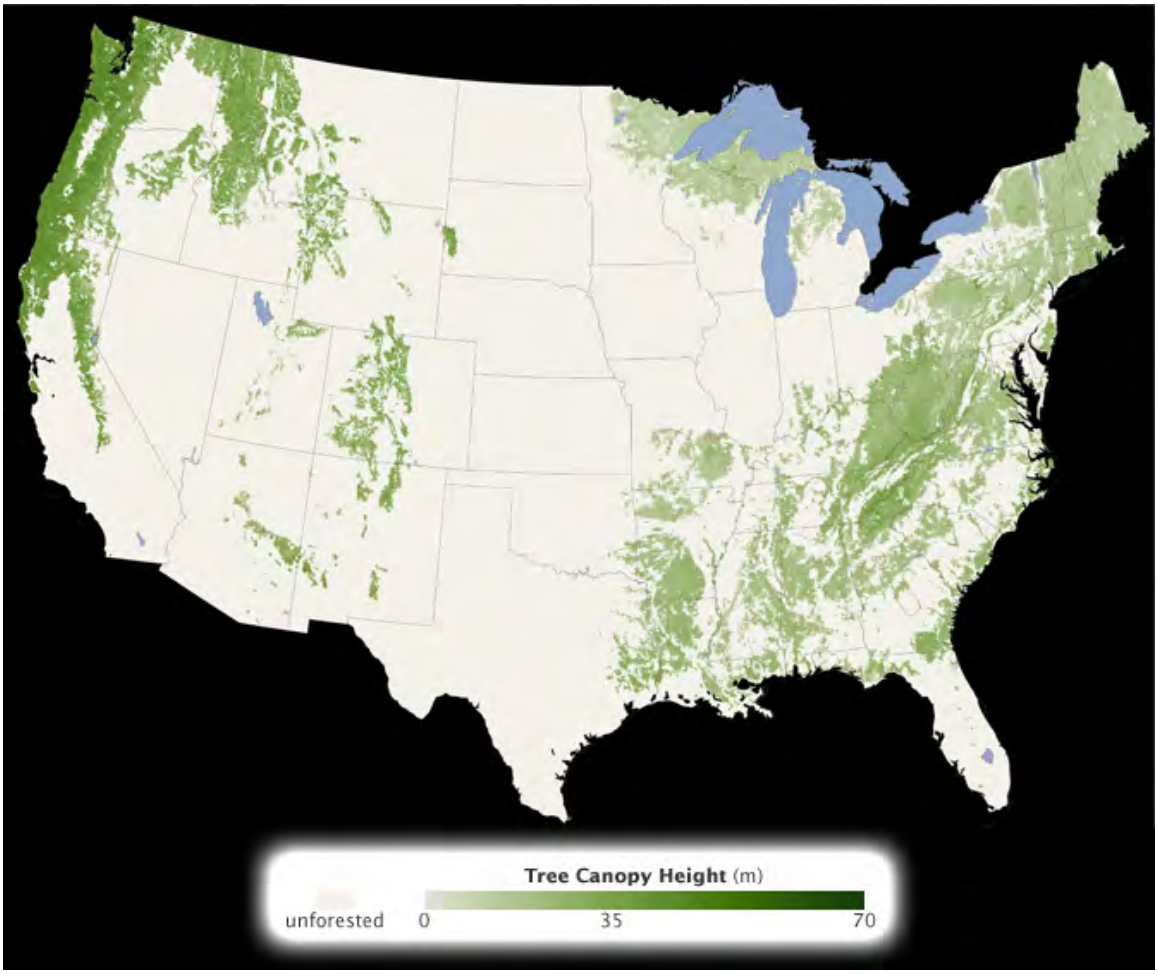

Figure 5. A forest canopy height map of the contiguous United States (From Lefsky, 2010)

Airborne laser scanning in recent years has developed into a powerful tool used with much success in the fields of engineering, archeology, and forestry (Vosselman & Maas, 2010). In these fields, airborne LiDAR systems have shown some clear advantages to traditional data collection methods. LiDAR has the capacity for high data

densities and good data accuracy. Some of the highest measurement densities are captured by helicopter mounted systems due to their slower airspeed and can take up to 30 measurements/m^2. Fast data acquisition is another advantage of airborne systems, as opposed to field measurements on the ground. Airborne LiDAR systems also require a minimal amount of ground truth. Field work is minimal since LiDAR generally only requires a few ground reference points, even for large data collection areas (Vosselman & Maas, 2010).

For engineering practices, airborne LiDAR systems are used in corridor mapping of outdoor structures such as railroads, power lines, pipelines, and dikes. For power line and railroad monitoring, LiDAR is useful to map and then model the immediate area surrounding the subject of interest. Vegetation growing too close can be identified and removed. For pipeline studies, terrain around the pipelines is studied to assess the impact and possible damage that could occur to the pipeline from the terrain. Dike and levee monitoring programs also use LiDAR to monitor and study the structure profiles as well as model the effects from potential failures. For example, in the aftermath of the collapse of two minor dikes in the Netherlands, the local Water Boards have used helicopter LiDAR systems, FLI-MAP, to regularly monitor over 6,500 kilometers of embankment (Franken & Flos, 2005).

In Detection and Vectorization of Roads from LiDAR Data, (Clode et al., 2007), road classification is conducted for urban terrain to support city planning and road network updating. They propose a method for automatic detection and vectorization of road networks solely from LiDAR data. For the purposes of their research, roads are assumed to be on the digital terrain model (DTM); that is, only the LiDAR points within a given tolerance of the DTM are considered as candidates for road. Next, a training algorithm, based on road intensity values, is used further classify roads in the scene. Morphological filtering is then conducted to remove gaps caused by overhanging trees or reflections from objects such as vehicles on the roads. At this point, the classified road images are vectorized using a convolution of the binary image with a phase coded disk (PCD). The road centerline, orientation, and width are determined by convolution with the PCD and then vectorized. Typical results are shown in Figure 6.

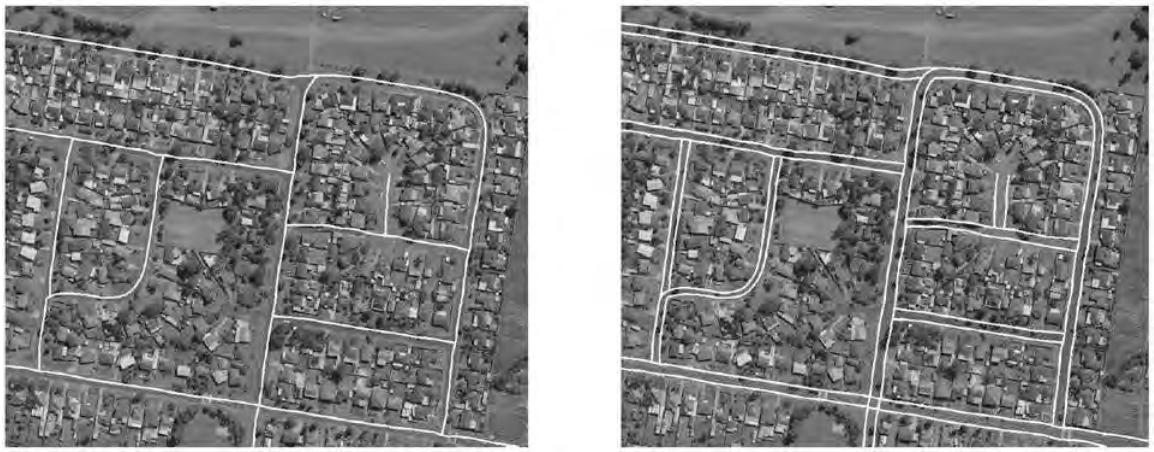

Figure 6. Fairfield, New South Wales, road centerline (left) and edges (right) are overlaid on aerial imagery to demonstrate results (From Clode et al., 2007)

Airborne LiDAR shows great promise as a tool to inspect archeological sites in forested areas. Woodlands can protect archeological remains from erosion, but also conceal archeological structures that could otherwise be identified from aerial photography. In these wooded areas, LiDAR can create detailed DTMs that have made important contributions to archeological prospection (Vosselman & Maas, 2010). The uses of LiDAR in archeological survey have some of the same considerations as using LiDAR to identify trails under tree canopy. To identify features beneath tree canopy, a high initial point density is required to ensure a sufficient number of pulse measurements are returned from the ground. In an archeological study of the Mayan City of Caracol the LiDAR collection, depicted in the figure below, consisted of two sets of perpendicular flight lines with 50% overlap, low operating altitude (800 m), and a high PRF (100 kHz) which resulted in an average of 20 returns per square meter (Diaz, 2011). This area has been heavily ground truthed and studied using traditional archeological survey techniques by researchers at the University of Central Florida since 1983. After comparisons of the LiDAR data to the ground surveys, the agreement was very good, and over the study area the LiDAR data showed higher spatial resolution identifying many new archeological features previously undiscovered by ground archeology teams (Diaz, 2011).

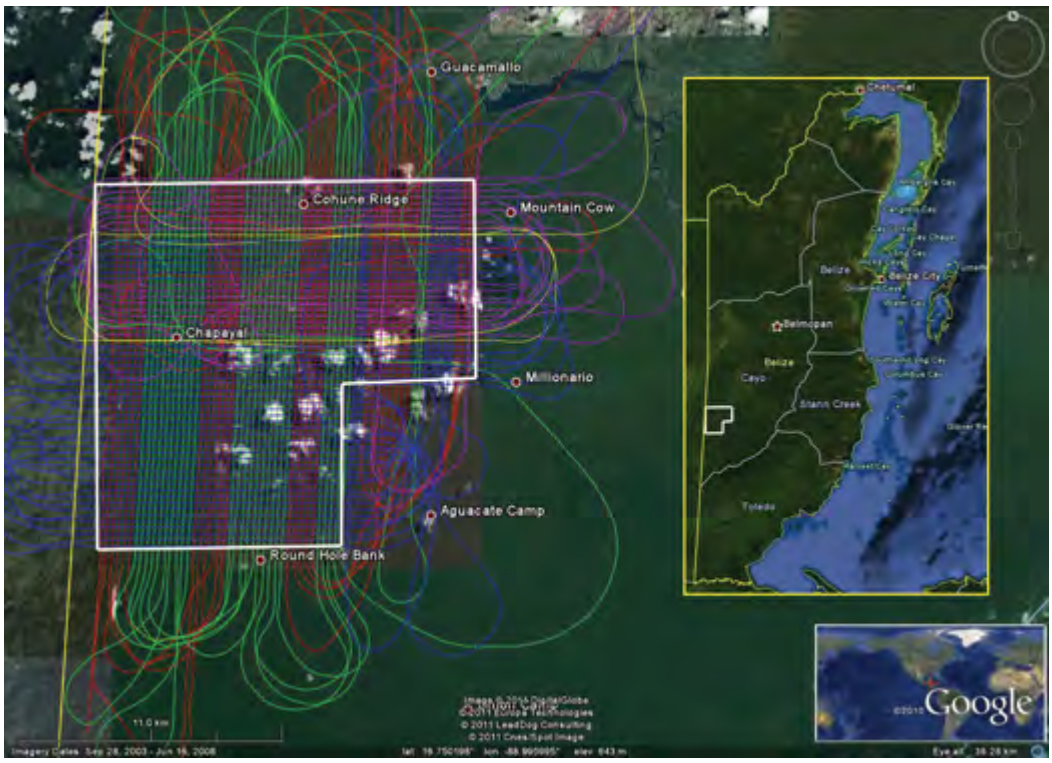

Figure 7. Map showing the Vaca Plateau project area in western Belize defined by the white box. The colored lines represent the ground tracks of the different flights (From Diaz, 2011)

An elegant treatment of LiDAR use in archeology was written by Crutchley and Crow (2010) for English Heritage, the United Kingdom's statutory advisor on the historic environment. They discuss LiDAR fundamentals, file format types, project planning, data manipulation, and interpretation. Of particular interest are the five case studies conducted and discussed. The case studies, which were conducted from 2005 through 2008, built upon each other going from a previously intensely studied area, Stonehenge, to a later project, Savernake Forest, which assessed the value of using LiDAR in a woodland environment (Crutchley & Crow, 2009). They found that by using bare earth hill shaded products with the maximum vegetation removed; previously unrecorded archeological monuments were identified for further ground study.

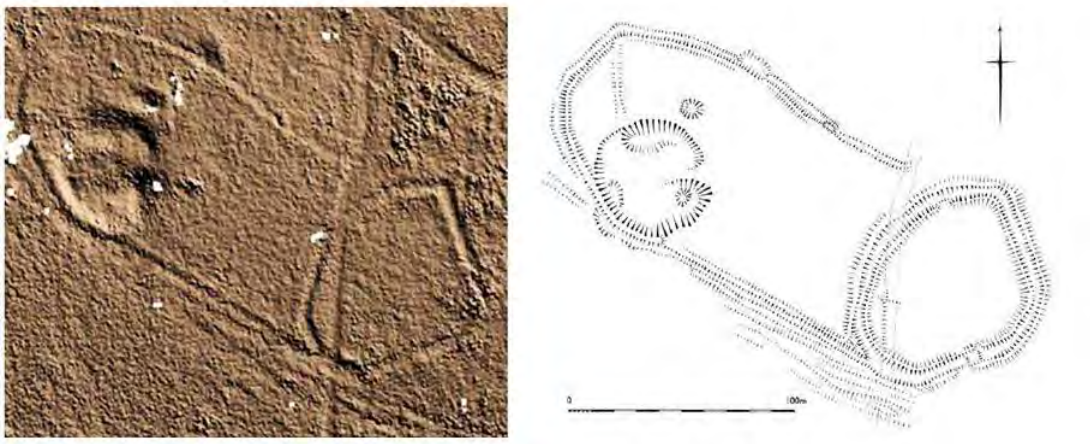

Figure 8. Enclosures at Church Walk from LiDAR (left) and ground survey (right) revealing almost exact agreement on size, location, and shape of archeological features (From Crutchley & Crow, 2009)

Since airborne LiDAR became commercially viable in the 1990s, foresters have used scanning systems and processes in the areas of forest management, inventory, carbon sink analysis, biodiversity characterization, and habitat analysis. Conventional means of conducting these studies involve physically walking the ground and taking key measurements; tree height, diameter, and volume, for a small representative plot and then extrapolating those results to include the entire stand of trees. These techniques have an estimated accuracy of only 15–30% (Vosselman & Maas, 2010). However, using LiDAR these same measurements can be accomplished to measure the same parameters for full-field rather than plot based forest inventories. Also, with increased point density available in modern systems, LiDAR can conduct measurements over a whole tree stand (requiring point spacing of 2–4 m) or can make measurements on a tree-wise approach for individual trees (requires more than one point per square meter).

Within the field of forestry, forest road planning and mapping plays an important role in management activities. Forest management professionals can use road inventory data to evaluate land use impacts, watershed disturbances, and future planning of forest road networks (White, 2010). Electro-optical satellite imagery and likewise aerial photography have not been effective methods for forest road mapping since even sparse tree cover prevents those sensors from observing the trails under canopy. Ground

inventories of forest roads are time consuming, expensive, and subject to much uncertainty. Across studies and estimates of forest service road systems, from 20% up to as much as 50% of road lengths are thought missing from inventories, and roads and trails in privately held lands are seldom inventoried or reported (R. A. White, Dietterick, Mastin, & Strohman, 2010). In their research, White et al. (2010) manually mapped a forest road beneath tree canopy to a positional accuracy of 1.5 m and road grade measurements within 0.53% of ground survey. Similarly, Espinoza and Owens (2007) demonstrated an 82% accuracy rate of covered trail identification from LiDAR derived products.

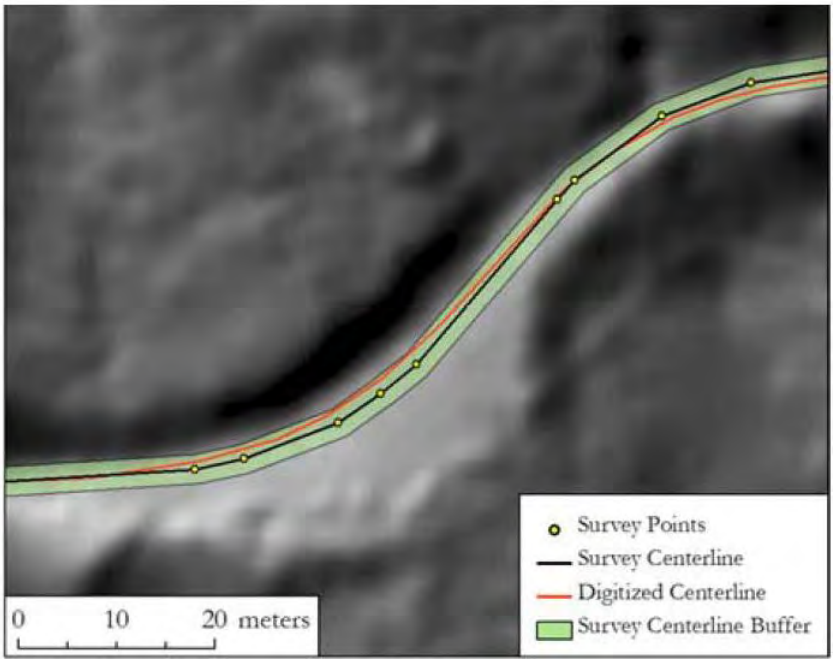

Figure 9. Field surveyed centerline (black) and digitized centerline (red) (From White et al., 2010)

David et al., 2009, attempt to automate the forest road detection process using only LiDAR data. Following a similar methodology as (Clode et al., 2007), the researchers use three LiDAR derived products to detect trails. The three products are a normalized digital surface model (nDSM), an altimetric variance image, and an intensity image. Using these three layers the researchers identified mean and variance for trails in each or the layers, and then used a region growing algorithm to expand trail sections from

a researcher selected seed. The resulting binary trail image is vectorized using morphological tools, and finally the trail borders and centerlines are exported as vector data. Results from their study are shown in Figure 10.

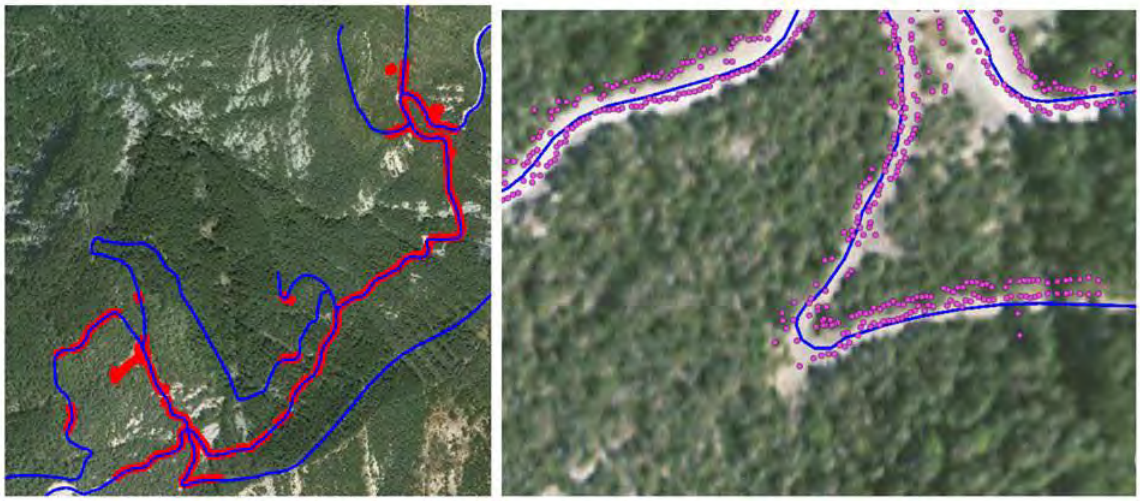

Figure 10. Results of pathway vectorization. Red is detected and vectorized pathways, pink are detected borderline points, and blue are pathways from an existing ground surveyed database (From David et al., 2009)

B. THEORY

1. Supervised Classification Techniques

The purpose of this research is to identify roads and trails under canopy. The advantage of LiDAR is its ability to "see to the ground" and derive digital terrain model (DTM) products to analyze. Once these products are created the problem of trail detection becomes an image processing problem, and several techniques, traditionally used on multispectral and hyperspectral images, can be applied to the LiDAR derived products. Supervised classification generally refers to a set of algorithms used to classify an image based on statistical analysis. Regardless of the statistical methods used, all classification techniques generally follow the same steps. First, decide on the number of classes the image is to be classified into, for this research the number of classes is two: trail and not trail. Second, pick a set of pixels in the image that represent the typical characteristics of the classes from step one. These pixels are known as the training data for the classifier (Richards & Jia, 2006). Third, this training data is used to determine the

parameters used for a probability model or some other set of equations that quantitatively describe the classes from step one. Next, using the trained classifier, label every pixel in the image as belonging to one of the classes from step one, from this produce class maps showing the results of the classification or produce the results in tabular form. Finally, compare the results of the class maps to ground truth obtained through site visits, survey data, of even by photo interpretation of the images. This process can be reiterated to improve classification results by refining the training data parameters based on knowledge of the original classes.

2. Maximum Likelihood Classification

Maximum likelihood classification is the most common type of supervised classification used with remote sensing images (Richards & Jia, 2006). This classification method is based on mean statistics; this method uses a Bayesian probability function that has been calculated from the training data classes. Then each pixel is judged as to which class it most probably belongs. The following approach is developed and explained in sufficient detail for most remote sensing applications by Richards (2006), but the process comes from the field of mathematical pattern recognition and machine learning, and is covered in greater mathematical detail in that discipline.

For each of the classes in the training data in the image

$$\omega_i, i = 1,...M$$

where M is the number of classes. To determine to which class a pixel vector **x** belongs the conditional probabilities are used.

$$p(\omega_i \,|\, \boldsymbol{x}), i = 1,...M$$

Vector **x** is a measurement of the brightness of a given pixel describing its location in multispectral space. The probability $p(\omega_i \,|\, \boldsymbol{x})$ is the likelihood that the class ω_i is correct for any given pixel at $\boldsymbol{x}$. At this point classification can be performed by

$$\boldsymbol{x} \in \omega_i, \text{ if } p(\omega_i \,|\, \boldsymbol{x}) > p(\omega_j \,|\, \boldsymbol{x}) \text{ for all } j \neq i$$

stating that a pixel at $\boldsymbol{x}$ belongs to class ω_i if $p(\omega_i|\boldsymbol{x})$ is the largest. However, $p(\omega_i|\boldsymbol{x})$ is unknown and must be computed by Bayes' theorem:

$$p(\omega_i|\boldsymbol{x}) = p(\boldsymbol{x}|\omega_i)\, p(\omega_i) / p(\boldsymbol{x})$$

where $p(\boldsymbol{x}|\omega_i)$ is estimated from the pixels in the training data, $p(\omega_i)$ is the probability that ω_i is in the image, and $p(\boldsymbol{x})$ is the probability of finding a pixel from any class at location $\boldsymbol{x}$, and can be computed by

$$p(\boldsymbol{x}) = \sum_{i=1}^{M} p(\boldsymbol{x}|\omega_i)\, p(\omega_i)$$

Since $p(\boldsymbol{x}|\omega_i)$ are known from the training data and $p(\omega_i)$ may be estimated from knowledge of the image it is more acceptable to perform the classification as follows:

$$\boldsymbol{x} \in \omega_i, \text{ if } p(\boldsymbol{x}|\omega_i)\, p(\omega_i) > p(\boldsymbol{x}|\omega_j)\, p(\omega_j) \text{ for all } j \neq i$$

In this expression $p(\boldsymbol{x})$ has been removed as a common expression.

To summarize, assuming the pixels in each class are normally distributed in multidimensional space, the maximum likelihood classifier computed both the variances and covariance of the training data when assigning pixels to one of the classes in the training data. Most image processing software allows the analyst to assign training sets and performs the above classification in the multidimensional space of the image. The above treatment will assign every pixel to one of the specified classes, however, if not all unique classes in an image were identified in the training data this may lead to a poor classification result (Richards & Jia, 2006). For this reason, many software packages also allow the analyst to set a threshold where any pixel below the threshold probability for all classes are not classified as depicted in Figure 11.

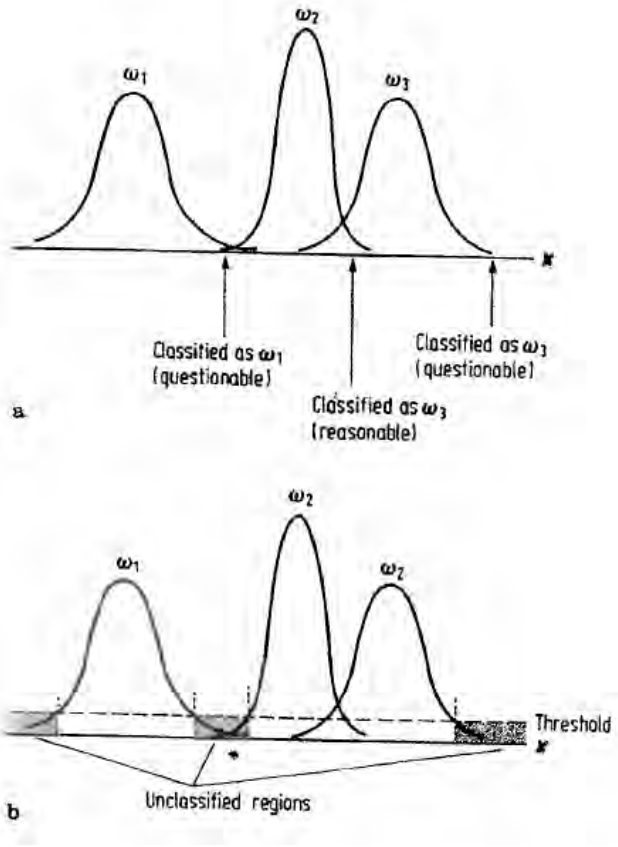

Figure 11. **a** Illustration of poor classification for patterns lying near the tails of the distribution functions for all of the classes; **b** Use of thresholds to remove poorly classified regions (From Richards & Jia, 2006)

3. Edge Detection and Enhancement

Another method explored in the course of this research was the use of neighborhood operations to enhance the trails in the LiDAR derived products. These procedures modify the brightness of an image pixel as a function of some weighted average of the brightness of the surrounding pixels (Richards & Jia, 2006). The methods attempted were template operators, where a box or window size is defined (template) and then moved over the original image row by row and column by column. The template is also known as the kernel. The operation takes the product of the pixel values of the

portion of the original image covered by the template and the template values, and these values are summed. The summed value is the new brightness value for the center pixel of the original image.

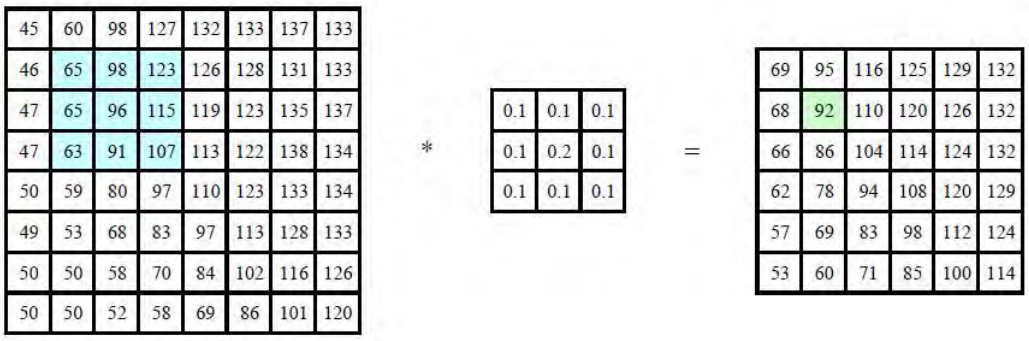

Figure 12. Neighborhood filtering (convolution): the image on the left is convolved with the filter in the middle to yield the image on the right. The light blue pixels indicate the source neighborhood for the light green destination pixel (After Szeliski, 2011)

These templates can be used to filter an image, adding blur, sharpening, enhancing edges, or removing noise in either color images or binary images as seen in Figure 13. For this research, several filters were experimented with, however, a Laplacian convolution filter was found to be most effective. It is a second derivative edge enhancement filter that operates without regard to the direction of the linear feature being enhanced. It uses a kernel with a high central value, typically negative values in the up-down and side-to-side directions, and values of zero on the corners of the filter.

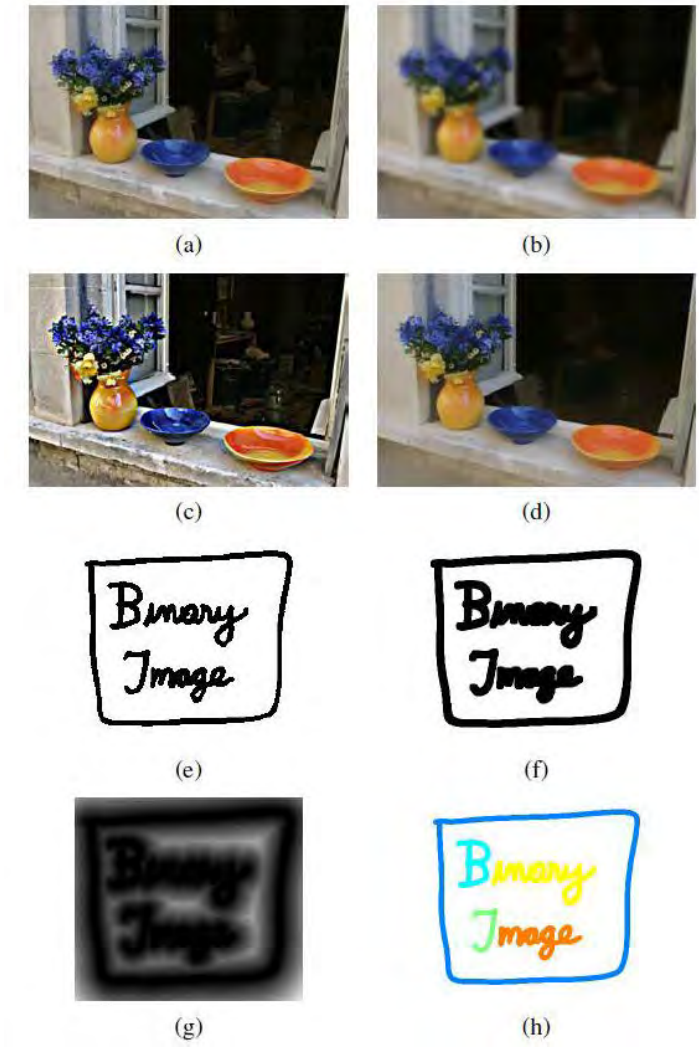

Figure 13. Examples of neighborhood operations: (a) original image; (b) blurred; (c) sharpened: (d) smoothed with edge-preserving filter; (e) binary image; (f) dilated; (g) distance transform; (h) connected components. For dilation and connected components, black pixels are assumed to have a value of 1 (From Szeliski, 2011)

4. Decision Trees

The above techniques are considered single stage classifications in that only one decision or operation is performed on a pixel. An alternate method is using a decision tree, where a series of binary decisions are made to determine the correct category for each pixel (Richards & Jia, 2006). The advantage to using the decision tree approach is

that at each level of the decision tree different data sets, different class attributes, and even different algorithms can be used to improve the accuracy of the overall classification of each pixel.

Using the decision tree process both the maximum likelihood classification and the edge enhancement can be performed on the same data set. Using a large to small approach, the maximum likelihood classification identifies all pixels that have the same characteristics are the trail training set. These trail pixels are labeled as the survivors of node one of the tree, those survivors move on to the next node of the decision tree where the previously described Laplacian edge enhancement filter can be applied only to the survivors mask from node one. The resulting survivors from node two have been identified as trail by both the maximum likelihood classification and the edge enhancement. At this point any erosion or dilation operators can be applied to the survivors from node two in order to reduce noise or enhance linear features, respectively.

III. PROBLEM

A. OVERVIEW

The location of the LiDAR data set for this study is in the Santa Cruz Mountains in California. Swanton Pacific Ranch is 19 km north of Santa Cruz and is owned and managed by California Polytechnic State University Corporation under the College of Agriculture, Food, and Environmental Sciences as an educational and research facility Swanton Pacific Ranch is a subset of the Scotts Creek Watershed, and the southern portion of the Little Creek Watershed is contained in Swanton Pacific Ranch. The topography of the study area is varied from the lower part of the property that is near sea level to the hills of the ranch that reach elevations of 488 m. The extent of the study area has an average slope of 45%.

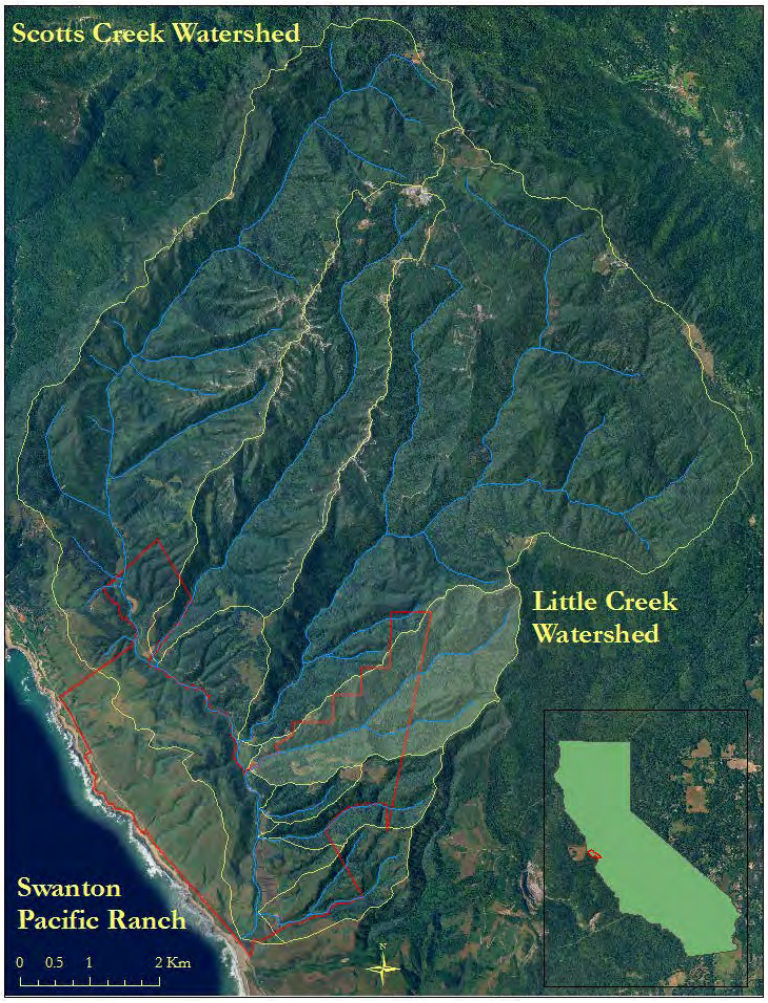

Figure 14. The Little Creek watershed, tributary to the Scotts Creek watershed. Swanton Pacific Ranch property boundary in red (From White, 2010)

The forest canopy in the study area consists primarily of second-growth coast redwood, but also has Douglas-fir and mature red alder. The overstory of the study has been measured using a vertical densitometer at thirty forest inventory locations throughout Swanton Pacific Ranch to support forest management. The canopy coverage at these sites range between 40 to 96% density, averaging 80% (White, 2010).

Figure 15. Overstory examples in Swanton Pacific Ranch over a forest haul road on left and over a foot trail on right

Typical roads and trails in the area range from forest hauls roads that follow former railroad grades to smaller foot trails that are approximately one meter wide. Examples of typical roads and trails identified on hillshade products are shown in Figure 16.

Figure 16. Typical road on left with 2 meter tape measure and typical trail on right with 1 meter tape measure

B. DATA SET AND COLLECTION METHOD

The primary data set for this research was contracted by Cal Poly, and flown by the Airborne 1 Corporation in March of 2010. The LiDAR system used was an Optech 3100/(EA) operating at 3,000 ft altitude above ground level (AGL) with a PRF of 150 kHz. The LiDAR survey parameters are summarized in Table 1.

Table 1. Swanton Pacific Ranch LiDAR collection parameters
(From Airborne 1, 2010)

LiDAR Survey Parameters	
Aircraft:	Navajo Chieftain
Sensor:	Optech 3100/(EA)
Altitude:	3,000 ft AGL
Scan angle:	14 degrees
Scan Frequency:	30 Hz
Pulse repetition frequency:	150 kHz
Returns:	4 per pulse (with intensity)

The extent of the LiDAR data covers approximately 11,200 acres, encompassing all of the Little Creek watershed, and Swanton Pacific Ranch property east of Scotts Creek, as shown in Figure 15. The data was delivered in the American Society for Photogrammetry and Remote Sensing (ASPRS) standardized format of LAS 1.1 files. The data set consists of 248 separate LAS files ranging in file size from 852 KB to 247 MB.

For this project the vendor, Airborne 1 Corporation, supplied all LAS files in the California State Plane Zone 3, NAD83 for the XY extent and NAVD88 for the Z extent, in U.S. survey feet. The advantage of using this is due to the relatively small area of study, the distortions in the state plane coordinate systems are less than Universal Transverse Mercator (UTM) or other common projections. However, through the course of the project and while working with multiple software suites to analyze the same dataset, some smaller analysis packages do not support state plane projections. To work around this, the data is analyzed in the smaller software package, for example QT Modeler by Applied Imagery, and those analysis results are then exported as either geotiffs or rasters, which can then be reprojected.

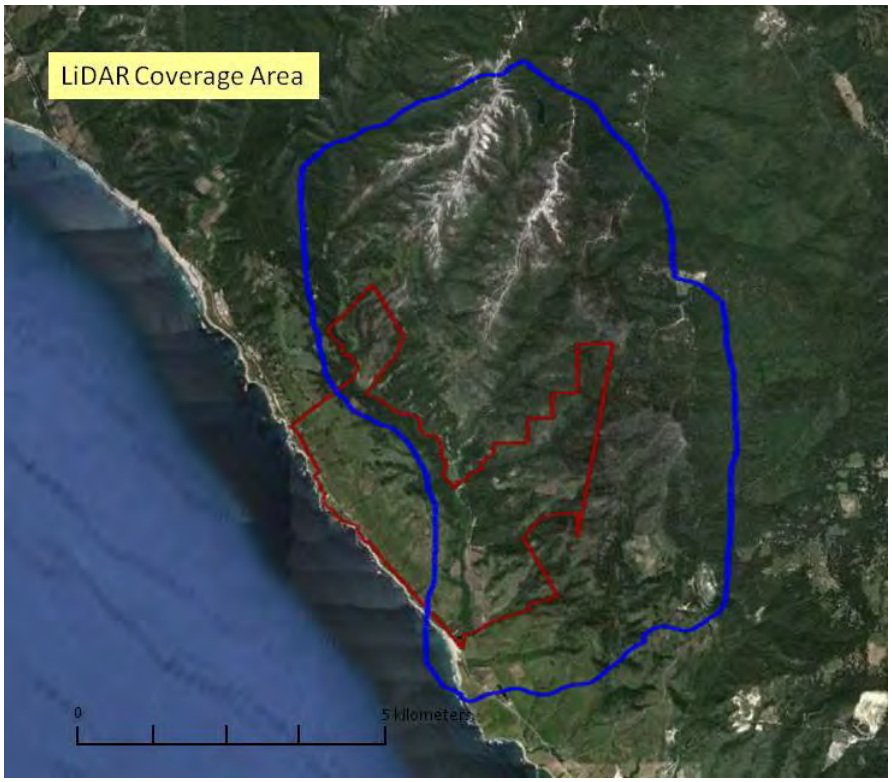

Figure 17. Swanton Pacific Ranch boundary in red and extent of LiDAR data coverage in blue (Imagery from Google Earth)

C. SOFTWARE USED

1. Economic and Social Research Institute (ESRI) ArcGIS

ArcGIS Desktop is a software product created by ESRI. It is used by many GIS professionals to compile, use, and manage geographic information in both a standalone version and for server enterprises (ESRI). ArcMap is one of the desktop products within the ArcGIS suite, and is used to construct maps, spatial analysis, and data compilation. The Swanton Pacific Ranch LiDAR data set was used with ArcMap version 10.0 to create a consolidated DEM from the 248 LAS files.

2. Environment for Visualizing Images (ENVI)

There are a number of different software suites for processing geospatial imagery. The classification and morphological operations for this thesis were conducted using ENVI from ITT Visual Information Solutions. ENVIs built-in topographic modeling,

classification, decision tree builder, and morphological operations were used to conduct analysis. Further explanation of the use of these tools is provided in the Methods and Observations Chapter.

D. FIELD EQUIPMENT

Table 2 summarizes the additional equipment used to collect ground truth data.

Table 2. Field equipment

Field Equipment	
Equipment	**Description**
Garmin GPSMAP 60CSX	Hand-held GPS receiver to collect ground track information and verify control point
Trimble Nomad	Outdoor rugged hand-held computer/GPS receiver to collect control points
Olympus Stylus 1030 SW	Digital camera to capture trail characteristics and overhead cover

THIS PAGE INTENTIONALLY LEFT BLANK

IV. METHODS AND OBSERVATIONS

A. DEM CREATION

The data set and point density were carefully evaluated for this research to ensure accurate results from products derived from the LiDAR point cloud, specifically ground point density as it affects the accuracy for DEMs and DSMs particularly under forest canopy. In ArcMap, the Point File Information tool under the 3D Analyst toolbox computes point spacing for each LAS file by comparing the size of the XY extent of the file to the file's point count. This tool works to quickly summarize large data sets since it can obtain all needed information from the LAS header. As seen in Figure 18, the data set for all returns ranges from 0.55 to 1.77 ft between points, with a mean of 0.77 ft. However, if only ground returns are considered, the point spacing increases to a range of 1.13 to 4.62 ft, with a mean of 1.99 ft.

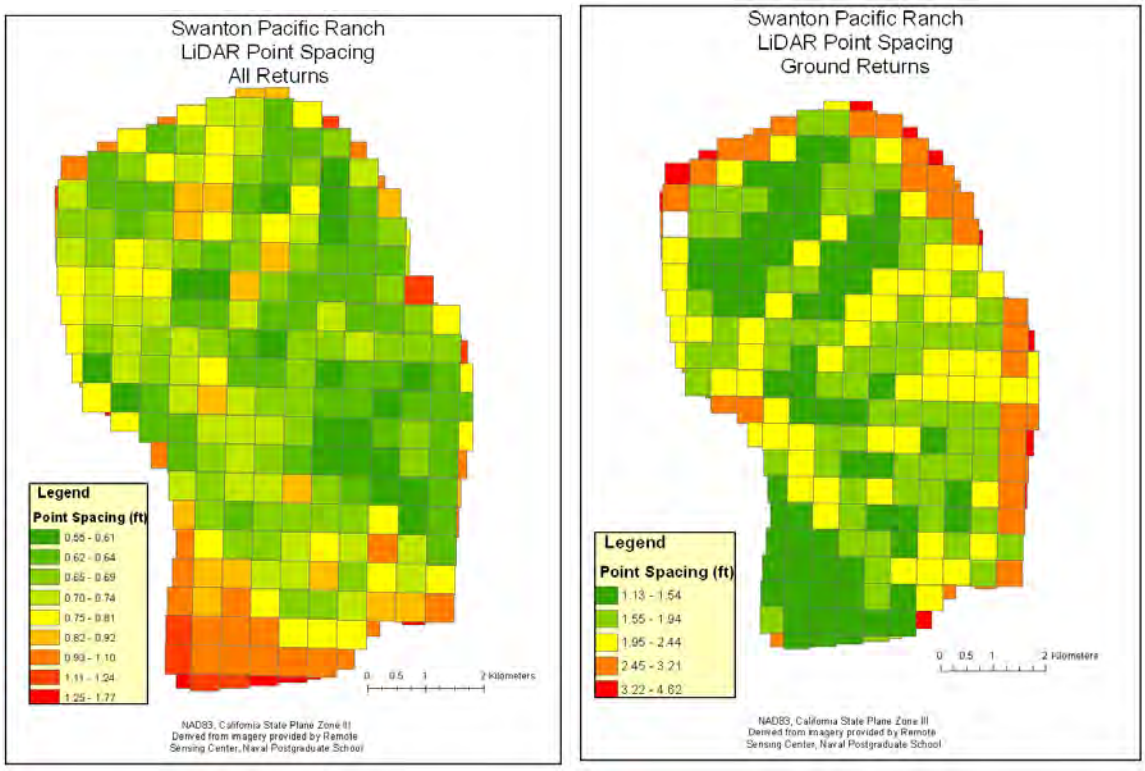

Figure 18. Point density comparison between all returns and only ground classified returns

At this point, sufficient point density exists to begin DTM creation. For DTM creation in ArcMap, the workflow begins by organizing the data in the 3D point cloud into a format that ArcMap can read (ESRI, 2010). To do this, convert the LAS files to a Multipoint Feature set using the LAS to Multipoint tool found in 3D Analyst → Conversion → From File. To build the terrain dataset only the ground classified points are used for the terrain wizard. The terrain wizard is found under a File Geodatabase → Feature Dataset, by right clicking and choosing New → Terrain. To create the DEM use the Terrain to Raster tool found in 3D Analyst → Conversion → From Terrain; creates the output DTM using the following parameters: Method: Natural_Neighbors, Cellsize: 3.28, and Pyramid Level: 0.

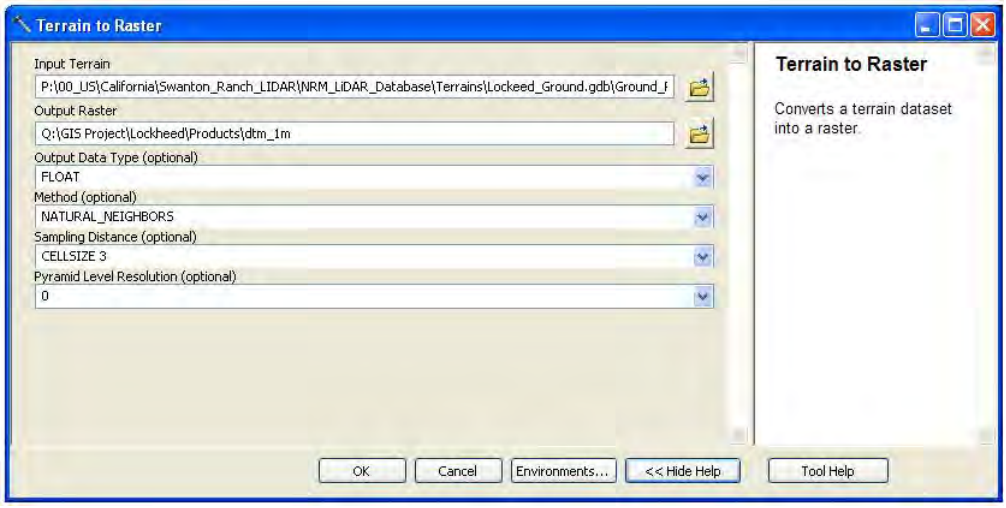

Figure 19. Terrain to Raster tool in ArcMap used for DTM creation of 1 meter resolution

Method refers to method of interpolation, and choices are natural neighbor or linear. These methods are TIN-based interpolation methods applied through the triangulated terrain surface. Natural neighbor, while not as fast as linear, generally produces better results in terms of accuracy. This method finds the closest set of input points to a query point and applies weights to them based on proportionate areas to interpolate a value (Sibson, 1981). The cell size sets the output resolution; for this example 3.28 produces a 1 meter resolution DTM since the original data set is in U.S.

feet. The resolution parameter indicates which pyramid level of the terrain dataset to use for conversion. To output a raster dataset at full resolution, this parameter is set to 0.

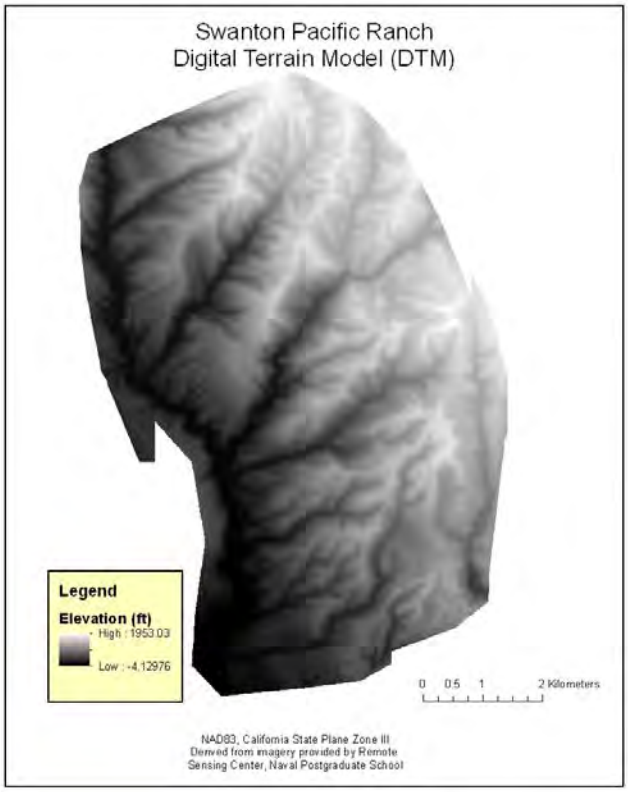

Figure 20. DTM at 1 meter resolution produced from LiDAR point cloud

B. CLASSIFICATION

The 1 meter DTM was imported into ENVI for characterization and classification of the data, specifically, defining trail parameters that could be observed from the DTM and DTM derived products. Using the ENVI Topographic Modeling tool from the main menu, the software computes statistics from the DTM and outputs 11 bands, each depicting a separate characteristic derived from the DTM as seen in Figure 21.

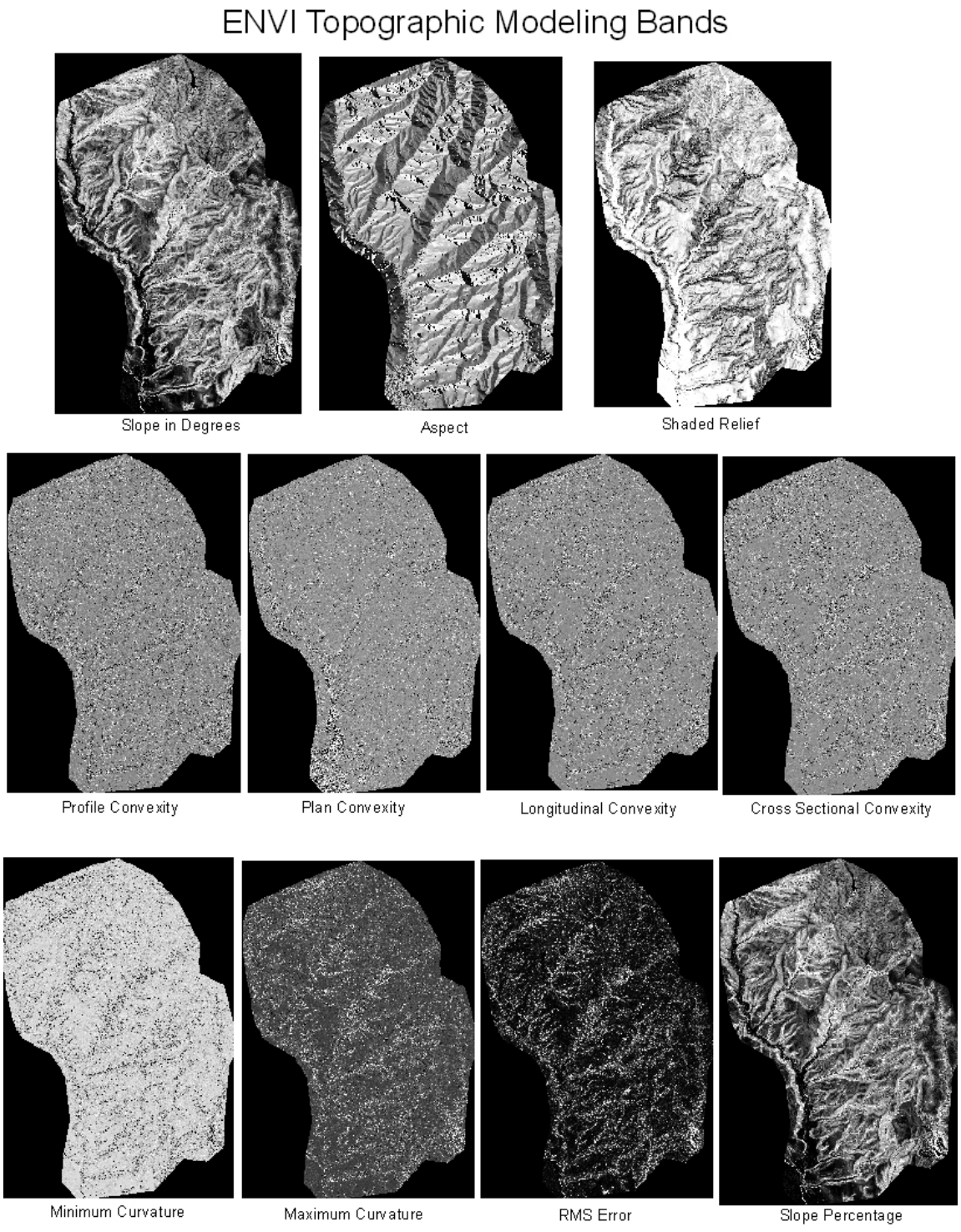

Figure 21. Full scene images representing the eleven bands created by the ENVI Topographic Modeling tool from a DTM

The topographic modeling tool in ENVI takes a DTM input and extracts parameters of the scene. ENVI calculates these parameters by fitting a quadratic surface to the DTM for a user entered kernel size and then taking the appropriate derivatives (ITT Visual Information Solutions, 2010). The kernel size of three was used for this research. The slope is measured both in degrees and percentage, with zero degrees corresponding to a horizontal surface, and slope percentage calculated by the formula: 100*rise/run. The aspect is the direction that a surface faces, and is calculated with zero degrees to the north and increasing clockwise. Several convexities are determined, and the profile and plan convexity measure the rate of change of the slope and aspect respectively. The longitudinal convexity is the measure of the surface curvature in the down slope direction, and the cross-sectional convexity is the measure of the surface curvature in the across-slope direction. The minimum and maximum curvatures are calculations for the overall scene surface, and the root mean square (RMS) error measure how well the quadratic surface fits the DTM data.

At this time, training data is identified in the scene that represents a typical section of trail under tree canopy. Within the scene a region of interest (ROI) is identified that includes pixels of trail and nontrail in the scene.

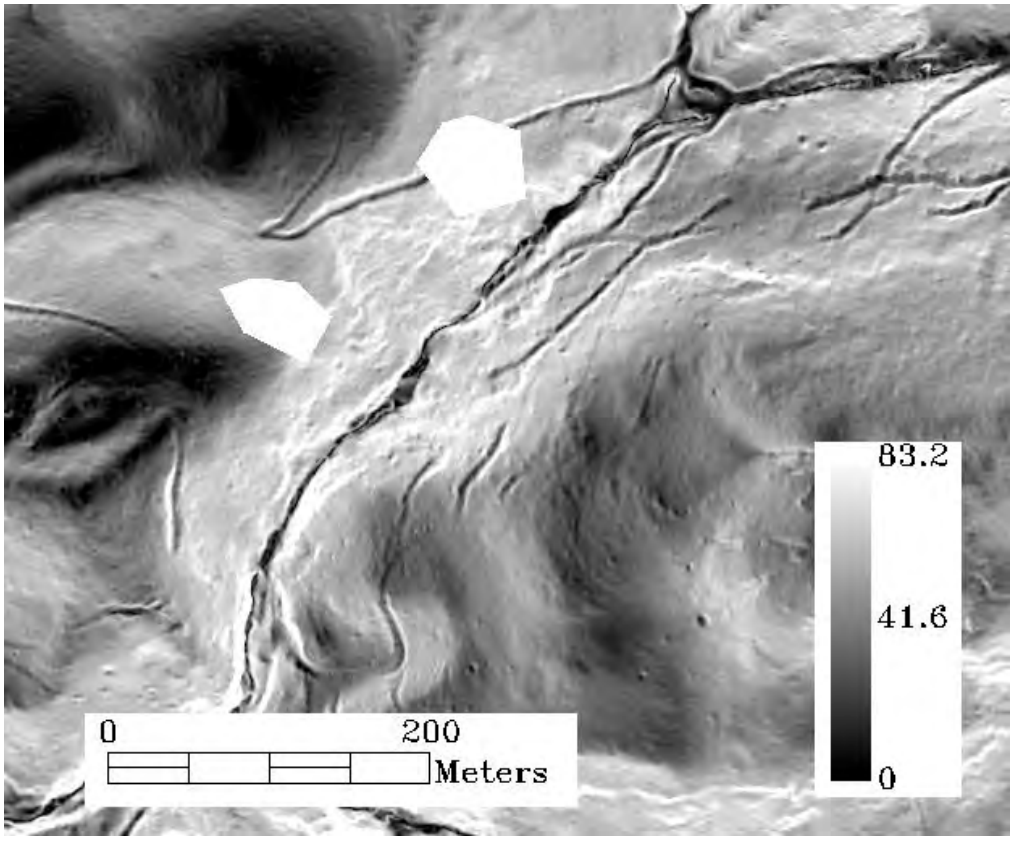

Figure 22. Initial ROIs (in white) to use as inputs for training data. Image depicts slope in degrees

The pixels contained in the ROIs were exported to the n-D visualizer. The n-D visualizer is used in spectral image analysis to locate, identify, and cluster the purest pixels and extreme spectral responses within a data set. For this research the n-D visualizer was used to check the separability of pixel clusters by visualizing the data cloud in n-D space using the image bands as plot axes. The data can be rotated, grouped into classes, and those classes can be collapsed to make finer classification easier.

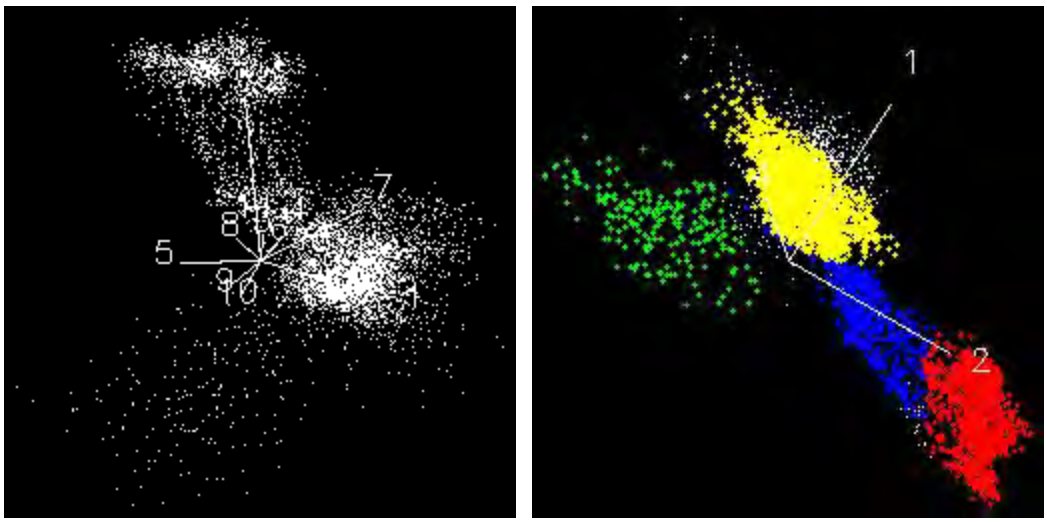

Figure 23. Initial ROI pixels plotted in n-D visualizer on left plotted in all eleven band axes, user clustered pixels in n-D visualizer on right plotted using bands 1, 2, and 4

The results of the used clustered pixel classes were then exported back to the image as new class ROIs. In this example, the green pixels represent training data pixels for trail; all other classes are considered not trail in red, blue, and yellow pixels.

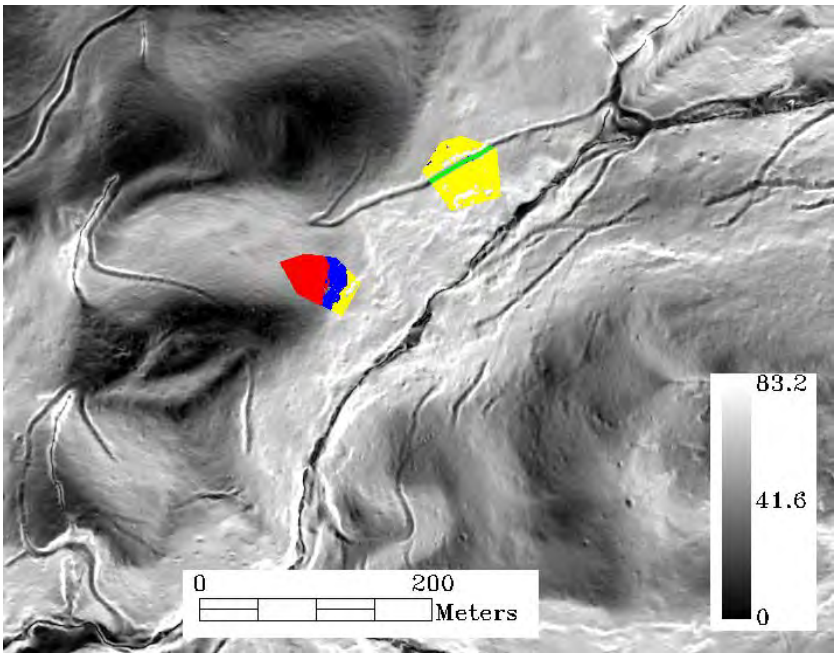

Figure 24. Clustered class ROIs overlaid on slope image, green pixels are trail and all other classes are not trail

Using 201 green pixels as the exemplar for a trail under canopy, out of a total of over 14 million pixels in the scene, supervised classification was conducted. Using maximum likelihood classification, the mean and variance for each class in Figure 24 is computed for each of the eleven bands. Then, each pixel is classified into one of the four classes to which it has the highest probability of belonging.

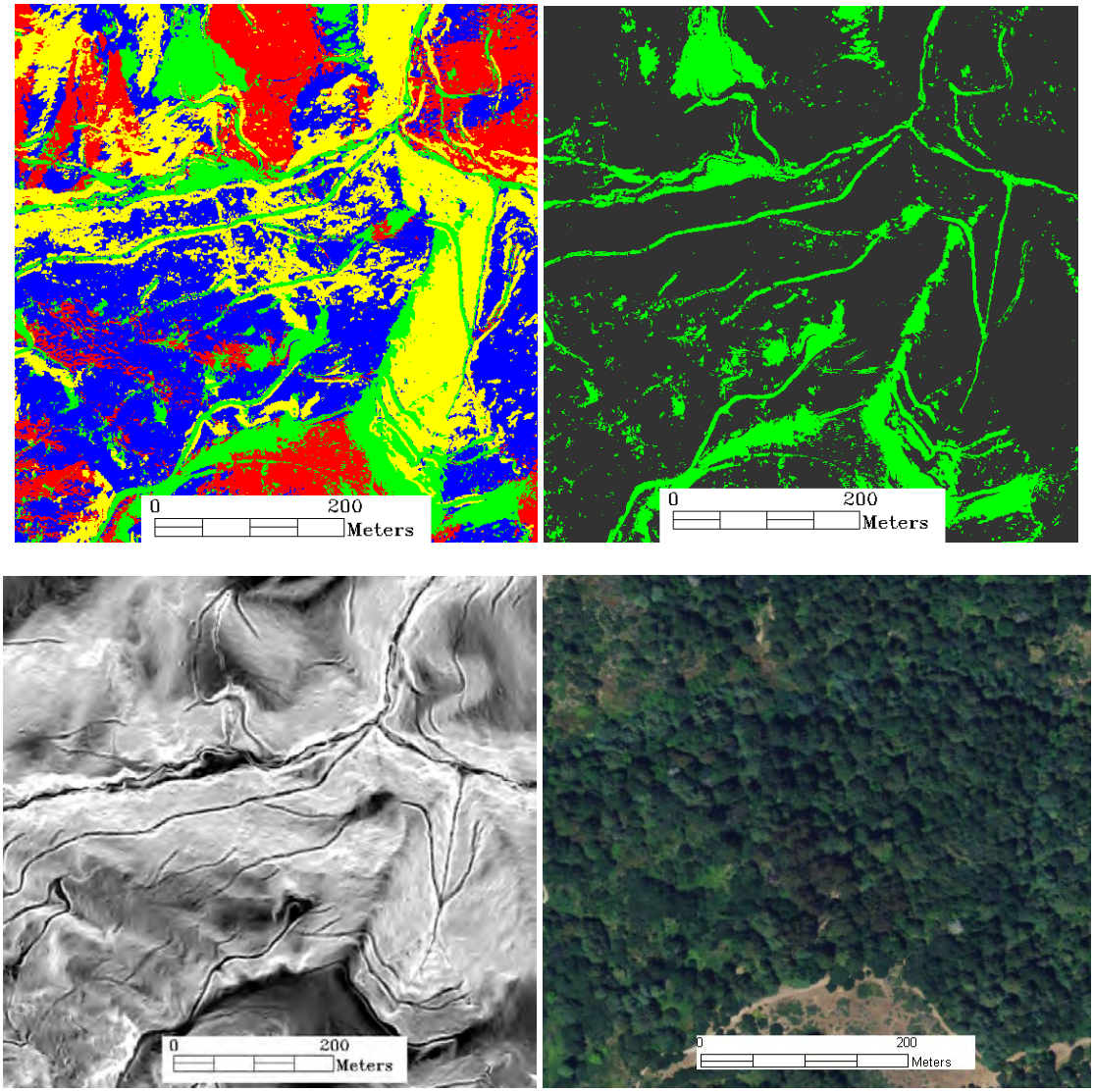

Figure 25. Result from maximum likelihood classification with all classes (upper left), same spatial subset with only trails identified in green (upper right), same spatial subset showing the slope in degrees band(lower left) and overhead imagery for comparison (lower right)

Rule images were generated during the classification process as well. The rule images show the classification results, before the final assignment of classes. For example, pixels in the rule image for n_D class #2 (Trail) for the maximum likelihood classifier represent the likelihood that it belongs to that class. A rule image for maximum likelihood classification is shown in Figure 26.

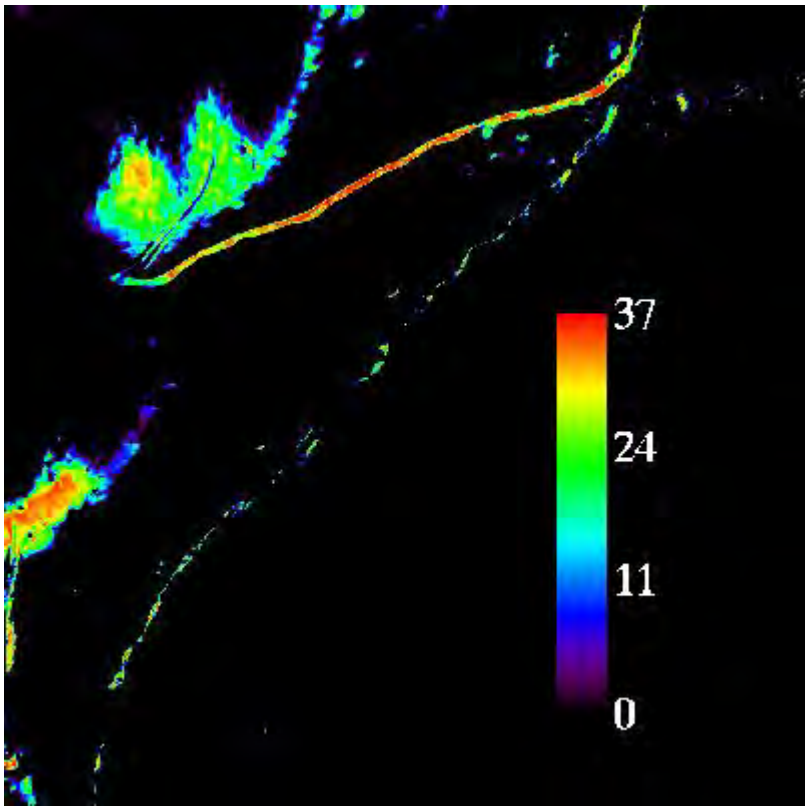

Figure 26. Rule image for trail classified pixels generated during maximum likelihood classification, higher values represent higher likelihood that pixel belongs to trail class. The upper portion of the image shows a trail segment, and the intermittent long diagonal corresponds to a stream bed.

Using the same procedures, several classification techniques were evaluated and compared. The evaluation and comparison will be further explained and discussed in Chapter V. ENVI provides nine supervised classification techniques that have been developed and used primarily for spectral classification of multispectral and hyperspectral imagery. Of these nine, four were chosen and evaluated for trail classification on the Swanton Pacific Ranch scene. Maximum likelihood classification as

discussed in Chapter II was chosen as the preferred method. Parallelepiped classification uses a decision rule to classify data. The decision boundaries form an n-dimensional parallelepiped classification in the image data space defined based on the standard deviation threshold from the mean of each class (ITT Visual Information Solutions, 2010). If the pixels in the scene fall within the threshold it belongs to that class, if it falls in multiple classes it is assigned to the last class matched, and if it does not fall within a threshold it is unclassified. The minimum distance classifier uses mean vectors for each training set, and calculates the Euclidian distance from each unknown pixel to the mean vector for each class in the training set. All unknown pixels are then classified to the closest vector from the training set classes. The Mahalanobis distance classification uses statistics for each class, similar to maximum likelihood classification, but assumes class covariances are the same so it is a faster method.

C. POST CLASSIFICATION FILTER METHODS

Post classification image processing techniques were applied to classified images to improve the accuracy of the final product. Convolution and morphology filters were investigated, both in combination and individually. ENVI also provides sieve and clump techniques that can be applied to classified image products. These were evaluated as well. The output results from each of the filters were evaluated and will be discussed in Chapter V.

The convolution filters produce images in which the brightness value of a given pixel is a function of some weighted average of the brightness of the surrounding pixels. The extent of the surrounding pixels considered by the convolution function can vary in size, and is known as a kernel. Median and Laplacian convolution filters were used in this research. Median filters smooth an image, removing regions of noise from an image smaller than the size of a user specified kernel. The Laplacian filter is a second derivative edge enhancement filter that is not dependant on edge direction.

Morphological operations in ENVI are dilation, erosion, opening, and closing. Dilate fills holes smaller than the user selected kernel in images, where erode removes small islands of pixels that are smaller than the kernel. Opening erodes the image

followed by dilation by the same size kernel. Opening is used to smooth contours, and remove islands and peaks in an image. Closing dilates an image followed by erosion, and is used to fuse narrow breaks and fill small holes.

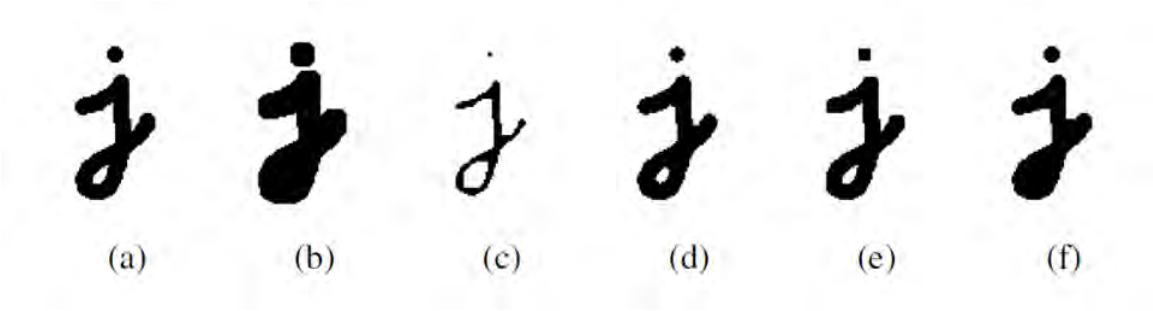

Figure 27. Examples of binary image morphology: (a) original image; (b) dilation; (c) erosion; (d) majority; (e) opening; (f) closing. Kernel size of 5x5 used for each. Majority was not used in this research, but rounds sharp corners (From Szeliski, 2011)

THIS PAGE INTENTIONALLY LEFT BLANK

V. ANALYSIS

A. METHODS OF EVALUATION AND ANALYSIS

To evaluate the different classification techniques and filtering methods a random sampling of pixels from the scene were selected. These pixels were ground truthed and then compared to classification images and filtered images to determine the performance of each method. This evaluation was conducted in two tiers. The first tier evaluated the four different classification techniques used: maximum likelihood, minimum distance, parallelepiped, and Mahalanobis distance. After evaluation, maximum likelihood was chosen as the best technique, and post classification filtering was conducted on maximum likelihood classifications only. The second tier of evaluations compared the performance of different filters and combinations of filters to each other.

To determine the number of pixels needed for a valid sampling, this study used the margin of error equation (De Veaux, Velleman, & Bock, 2009):

$$ME = z^* \sqrt{\frac{\hat{p}\hat{q}}{n}}$$

Where z* is 1.96 for a 95% confidence level, p=0.5 to determine the largest sample size regardless of the true proportions, and ME is set at 0.06. The equation is then:

$$0.06 = 1.96\sqrt{\frac{(0.5)(0.5)}{n}}$$

$$\sqrt{n} = \frac{1.96\sqrt{(0.5)(0.5)}}{0.06}$$

$$n = (16.3)^2 = 266.8$$

For this research this value was rounded up, and 300 pixels were randomly selected by the ENVI post classification random sample generator. The points were selected from a spatial subset of Swanton Pacific Ranch that is forested and has many roads and trails, as seen in Figure 28.

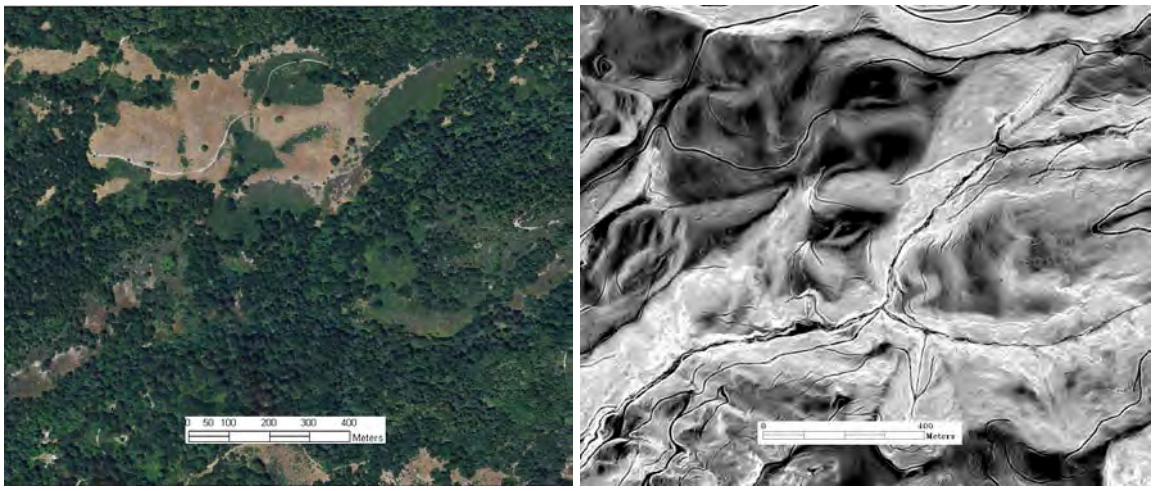

Figure 28. Spatial subset of random sampling. Imagery (on left) provided by NPS Remote Sensing Center and ENVI slope product (on right)

Each of the points were classified as trail or not trail using a combination of ground truth survey and DEM products. The sampling followed the color conventions from the classes identified in the training set, with green points corresponding to trail classified points and red, blue, and yellow corresponding to a not trail classification. Of the 267 points generated, after ground truth, 61 points were classified as trail and 206 were classified as not trail. The full list of points is in the Appendix, but the point breakdown summary was as follows:

Table 3. Random point sampling summary

ROI name:	**ROI rgb value:**	**ROI npts:**
Random Sample (first_attempt_topo15July / [Green] 201 points)	{0, 255, 0}	117
Random Sample (first_attempt_topo15July / [Red] 1228 points)	{255, 0, 0}	46
Random Sample (first_attempt_topo15July / [Blue] 585 points)	{0, 0, 255}	65
Random Sample (first_attempt_topo15July / [Yellow] 2616 points)	{255, 255, 0}	39

Using the same 267 points, each of the classification techniques and filtering methods were compared to the ground truth to evaluate performance. Performance was

measured using receiver operator characteristic (ROC) graphs for a discrete classifier. The thematic products from each of the processes in this research result in a classification into one of only two classes. With a discrete two class classifier and an instance (known as ground truth), there are four possible outcomes (Fawcett, 2004). If the instance is positive (trail) and it is classified as trail, it is counted as a true positive; if it is negative (classified not trail), it is counted as a false negative. If the instance is negative (not trail) and it is classified as negative it is counted as a true negative; if it is classified as positive it is counted as a false positive. Given these four categories a 2 x 2 confusion matrix can be constructed and forms the basis of many commonly used metrics as seen in Figure 29.

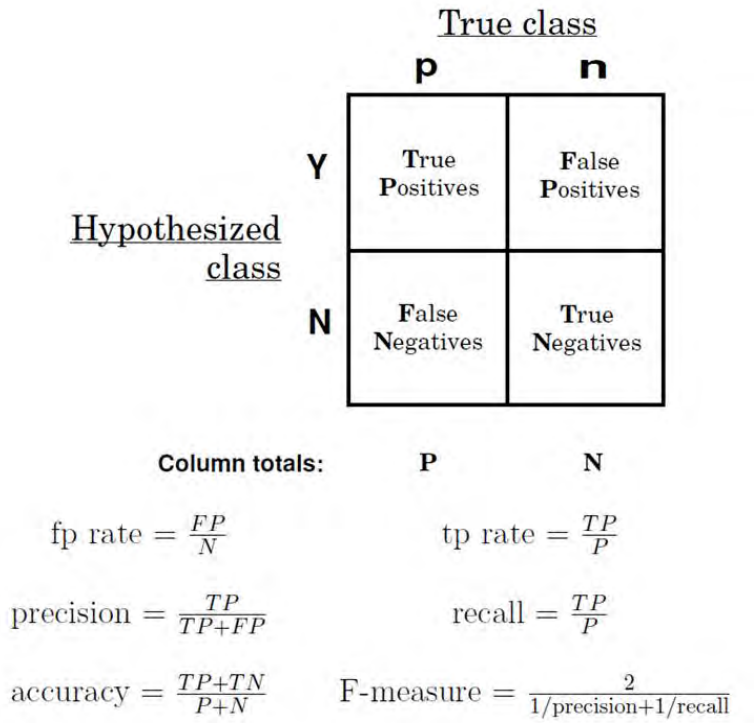

Figure 29. Confusion matrix and common performance metrics calculated from it (From Fawcett, 2004)

Using the metrics from Figure 28, ROC graphs are plotted with the TP rate on the Y axis and the FP rate on the X axis. Generally, one point in ROC space is better than another if it plots in the upper left of the graph, that is, it has a high true positive rate and low false positive rate. Classifiers on the left side of the graph with low false positive

rates make positive classifications only with strong evidence. Alternatively classifiers on the upper right side of the graph classify nearly all positives correctly, but have high false positive rates. A diagonal line where x=y, corresponds to random guessing.

B. EVALUATION OF CLASSIFICATION TECHNIQUES

Four classification techniques were evaluated using true positive rates and false positive rates as measures of effectiveness. Higher true positive rates and lower false positives rates are better for each discrete classifier. Each of the four classification techniques rely on the statistics of the training set to make a determination as to which class a pixel belongs, as discussed in Chapter IV. The training set mean, band list with description, and standard deviations are provided in Tables 4 through 7.

Table 4. Training set mean for each topographic modeling band by class

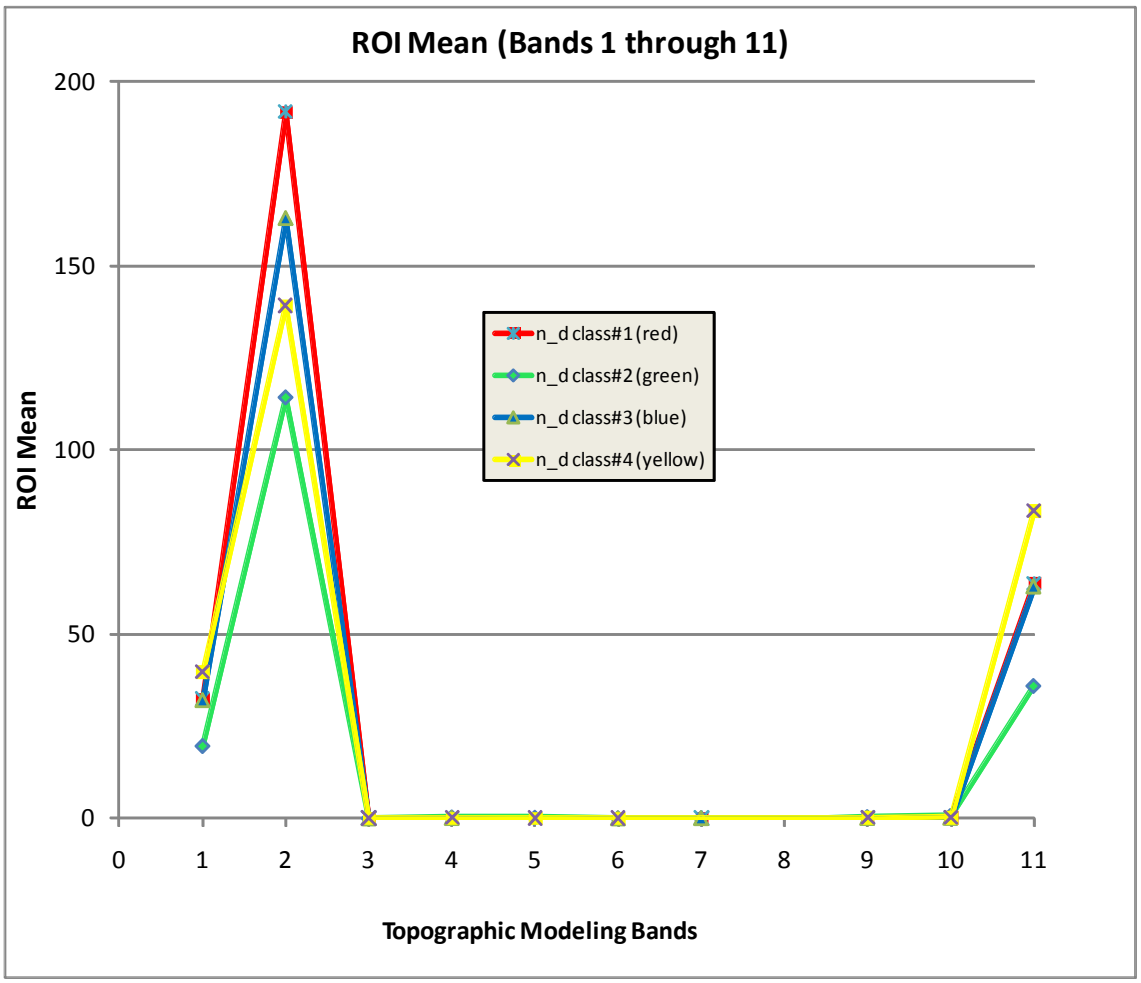

Table 5. Training set mean for topographic modeling bands 3 through 10 by class

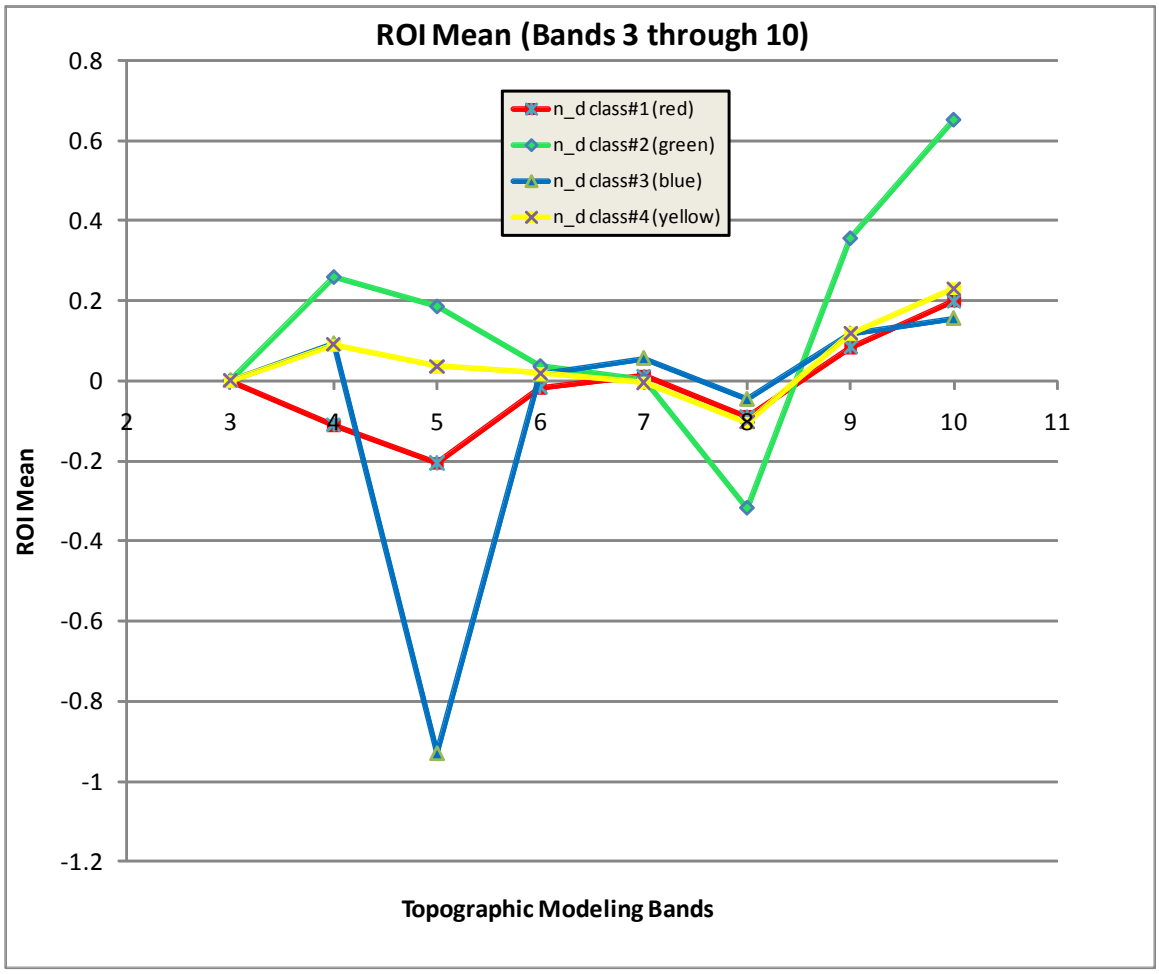

Table 6. Topographic Modeling band list

Band	Name	Description
1	Slope	Convention of 0 degrees for a horizontal plane
2	Aspect	The direction (azimuth) that a surface faces, in degrees clockwise from North (0 deg)
3	Shaded Relief	Renders terrain in 3D by use of shadows that would be cast by the sun from the NW
4	Profile Convexity	Rate of change of the slope intersecting with the plane of the z-axis and aspect direction
5	Plan Convexity	Rate of change of the aspect intersecting with the x,y plane
6	Longitude Convexity	Measures of the surface curvature orthogonally in the down slope direction
7	Cross Section Convexity	Measures of the surface curvature orthogonally in the across slope direction
8	Minimum Curvature	Minimum overall surface curvature
9	Maximum Curvature	Maximum overall surface curvature
10	RMS Error	Indication of how well the quadratic surface fits the digital elevation model
11	Slope Percentage	The percentage or degree change in elevation over distance

Table 7. Training set standard deviation for all topographic modeling bands by class

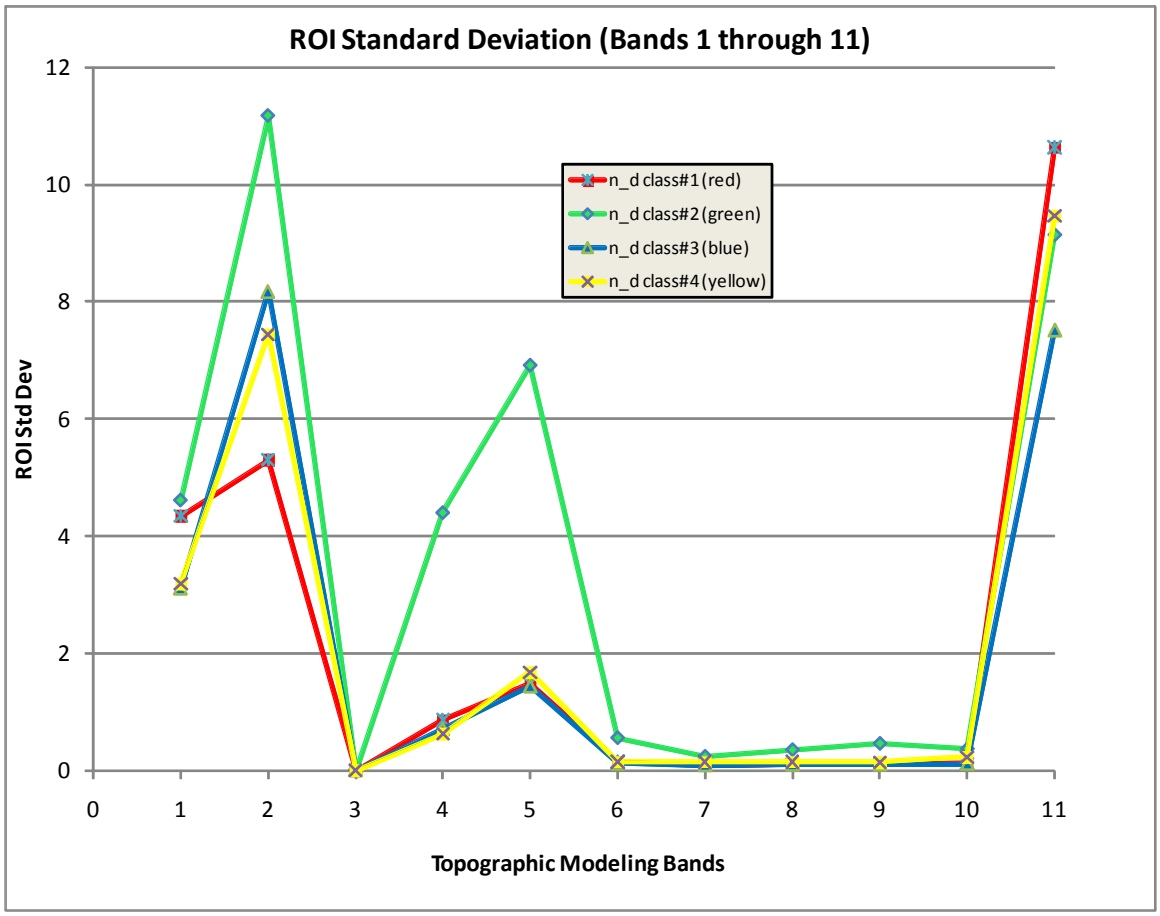

The Mahalanobis distance classifier had the lowest false positive rate of the four classifiers with 23.7%. It ranked three out of four for true positive rate with 67.2%.

Mahalanobis Distance

Classified as	Ground Truth: trail	Ground Truth: not
trail	41	49
not	19	158

fp rate =	23.7%
tp rate =	67.2%
precision =	45.6%
accuracy =	74.3%

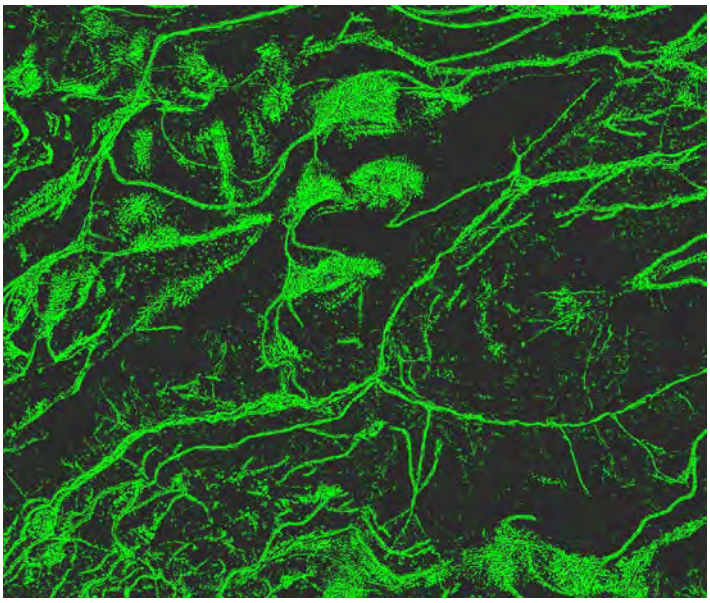

Figure 30. Mahalanobis distance confusion matrix with metrics and thematic map showing trails in green

The maximum likelihood classifier had the best true positive rate at 83.6%, and ranked two out of four for false positive rate with 31.9%.

Max Likelihood

Classified as	Ground Truth: trail	Ground Truth: not
trail	51	66
not	9	141

fp rate =	31.9%
tp rate =	83.6%
precision =	43.6%
accuracy =	71.6%

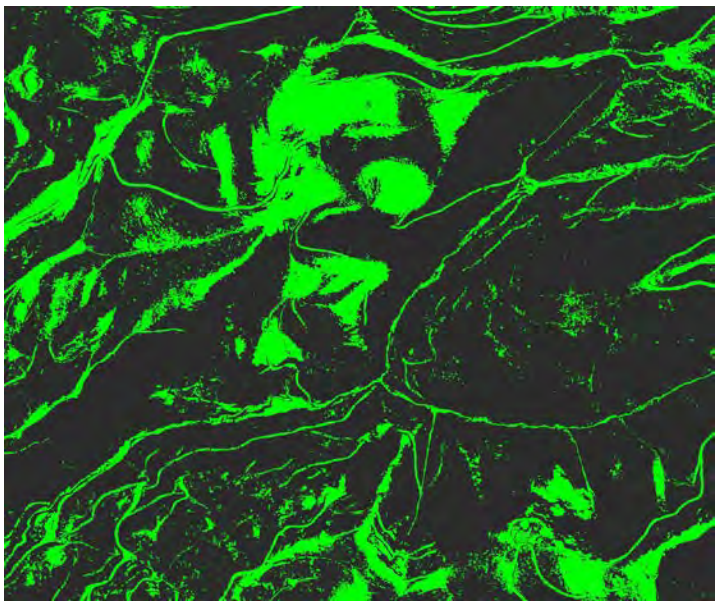

Figure 31. Maximum likelihood confusion matrix with metrics and thematic map

The minimum distance classifier had the second highest true positive rate with 83.6%, and also had the highest false positive rate with 51.7%.

Minimum distance

Classified as	Ground truth: trail	Ground truth: not
trail	51	107
not	9	100

fp rate =	51.7%
tp rate =	83.6%
precision =	32.3%
accuracy =	56.3%

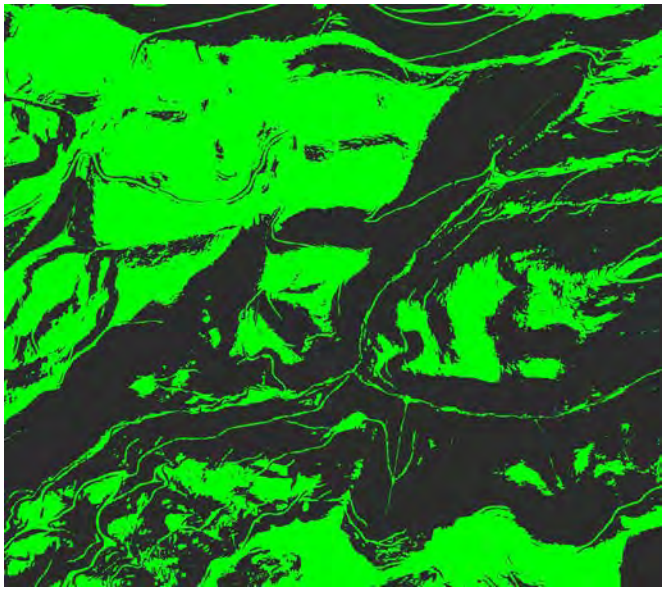

Figure 32. Minimum distance confusion matrix with metrics and thematic map

The parallelepiped classifier had the lowest true positive rate with 63.9%, and had the second highest false positive rate with 37.2%.

Parrallelepiped

Classified as	Ground truth: trail	Ground truth: not
trail	39	77
not	21	130

fp rate =	37.2%
tp rate =	63.9%
precision =	33.6%
accuracy =	63.1%

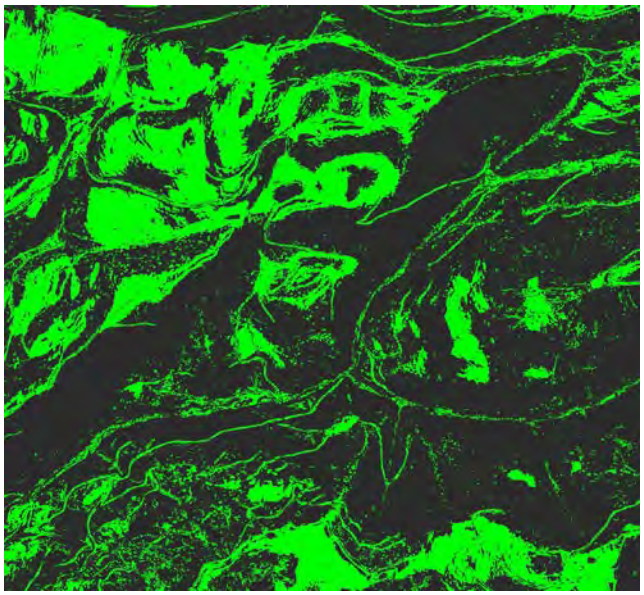

Figure 33. Parallelepiped confusion matrix with metrics and thematic map

The maximum likelihood classifier was chosen as the best classification technique in this instance due to its high true positive rate, and when graphed in ROC space in Table 8. The Mahalanobis distance classifier was ranked second over the minimum distance and parallelepiped classifiers due to its lower false positive rate. For the remainder of the research, the maximum likelihood classifier results were used to evaluate different filtering methods.

Table 8. Graph for classification techniques

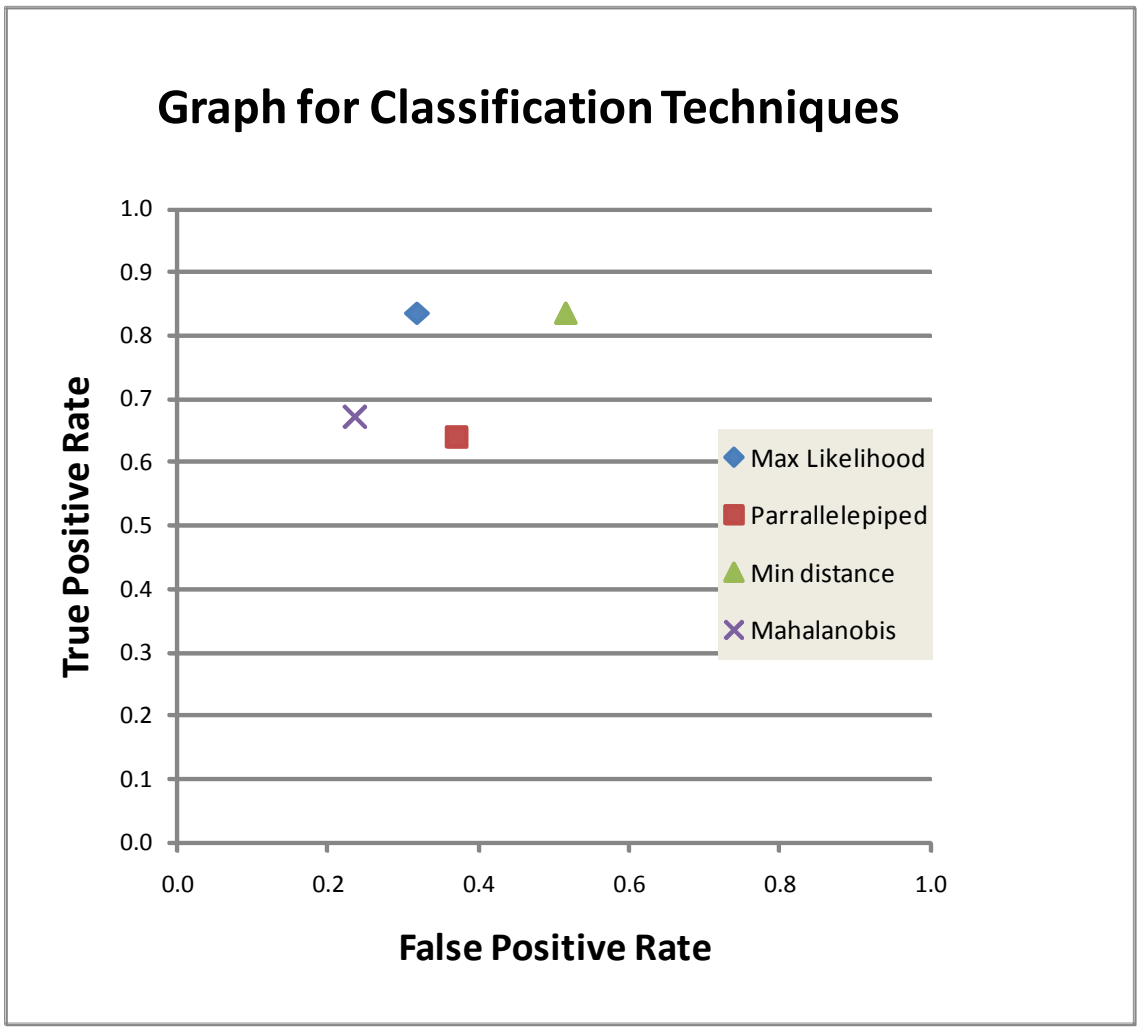

C. EVALUATION OF IMAGE PROCESSING METHODS

The same evaluation techniques were applied to the resulting products from the different image processing methods. Generally, three different approaches were applied to the maximum likelihood classified image. The first approach was to apply a median filter to remove noise in the image followed opening, closing, erosion, and dilation operators of varying structural size and comparing the results. The second approach was to use a post classification tool in ENVI named sieve and clump. The sieve function removes isolated pixels using blob grouping (ITT Visual Information Solutions, 2010). The function looks at local neighborhood for each pixel and determines if the pixel is grouped with pixels of the same class, if not it re-labels the pixel unclassified. The clump function groups together similarly classified areas after they have been sieved. The third approach used a decision tree to create a final product. Using the decision tree the first node separates trail classified points from non trail classified points. The second node of the decision tree takes the trail classified points, known as node one survivors, and applies a Laplacian edge detector. The output from this approach represents the intersection of the survivors from both nodes of the decision tree in a binary mask.

The naming conventions used attempt to capture the image processing method used as well as the size of the structuring element. This was done in an effort to aid further work, for example an image that has a median filter applied with a 5 x 5 kernel followed by the morphological operation closing with a 3 x 3 kernel would be labeled: median5by5_closing3by3. The sieve and clump products follow a similar naming convention, and all decision tree products start with the survivormask and follow the naming conventions for any processing that was applied to that mask. A summary of the image processing techniques used and their respective metrics are listed in Table 9.

Table 9. Image processing techniques used with performance metrics

Method	true pos	false pos	tru neg	false neg		tp rate	fp rate	precision	accuracy
max_likelihood	51	66	141	9		0.836	0.319	43.6%	71.6%
median5by5	51	66	141	9		0.836	0.319	43.6%	71.6%
median5by5_opening3by3	51	66	141	9		0.836	0.319	43.6%	71.6%
median5by5_closing3by3	50	66	141	10		0.820	0.319	43.1%	71.3%
median5by5_closing5by5	41	65	142	19		0.672	0.314	38.7%	68.3%
median5by5_erode3by3_dilate7by7	32	64	143	28		0.525	0.309	33.3%	65.3%
median5by5_erode7by7_dilate3by3	48	71	136	12		0.787	0.343	40.3%	68.7%
sieveAllclasses_clumpAllclasses	52	66	141	8		0.852	0.319	44.1%	72.0%
sieveAllclasses_clumpgeen	52	67	140	8		0.852	0.324	43.7%	71.6%
survivormask	15	9	198	45		0.246	0.043	62.5%	79.5%
survivormask_median3by3	14	4	226	56		0.230	0.019	77.8%	89.6%
survivormask_median3by3_3cyclesclosing	20	7	223	50		0.328	0.034	74.1%	90.7%

The image processing techniques only increased true positive rates in the sieve then clump processes, however, only slightly correctly identifying only one additional trail point than the original classifier. The most accurate processes were the products from the decision tree. All three decision tree products reduced the false positive rate to less than 5%, with the best performer with regards to accuracy being the decision tree product, followed by a median 3 x 3 filter, followed by 3 cycles of closing with a 3 x 3 filter. This process works the best since it moves from the more liberal classification process and step-by-step removes unwanted artifacts based on trail characteristics. The maximum likelihood classification identifies a high percentage of trails in the scene with an 83.6% true positive rate. The Laplacian convolution enhances edges of long linear features (trails) without regard to direction, and the decision tree survivors are those pixels that are both classified as trail and have edges. This product is smoothed with a median filter to remove noise in the scene while preserving edges, and finally the closing fuses any narrow breaks and fills small holes in the trail segments. The thematic map from this process is shown in Figure 34.

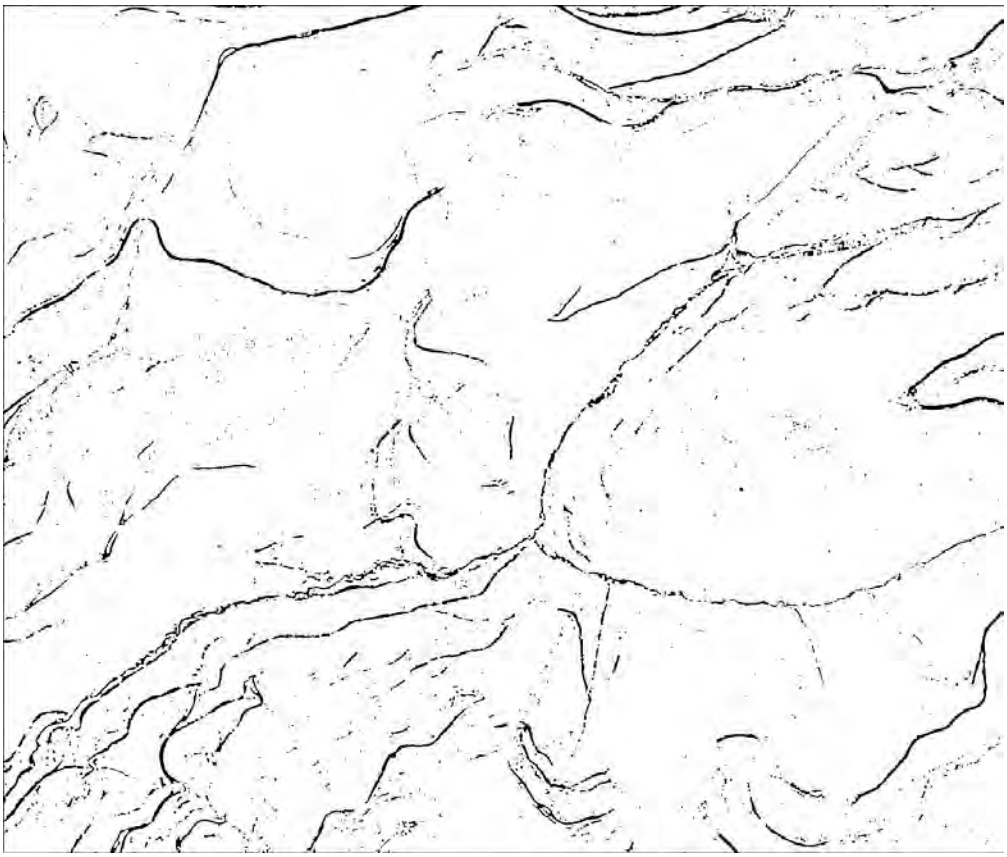

Figure 34. Binary image showing trail classified points in black from image processing

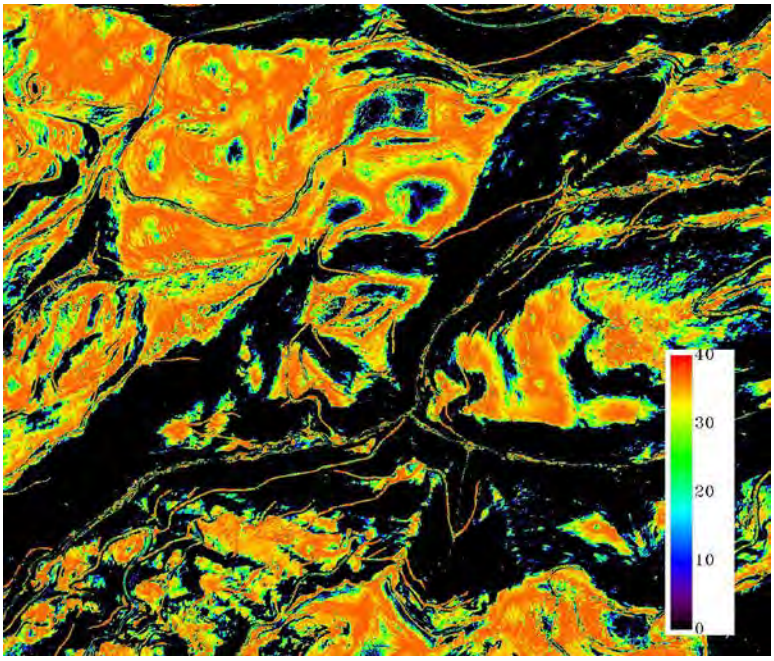

Figure 35. Rule image for same spatial subset as Figure 34 prior to image processing

VI. SUMMARY

The overall result of this experiment represented by the analysis in Chapter V is very encouraging that the process of statistical classification followed by image processing can correctly identify roads and trails under canopy using LiDAR. The point densities of current LiDAR systems are capable of penetrating second growth forest canopy, and producing accurate digital terrain models (DTMs). In this data set the slope values, convexities along different planes, and curvatures provided sufficient statistics to characterize unpaved road and trail segments within the study area. Supervised classification techniques traditionally used in remote sensing on multispectral and hyperspectral images were applied successfully to identify roads and trails after training data was identified.

Four classification techniques were used in the experiment to identify the best techniques for classifying roads and trails in forested areas. Among maximum likelihood, Mahalanobis distance, minimum distance, and parallelepiped classifiers maximum likelihood produced the highest true positive rate and was chosen as the sole classifier to conduct image processing. However, the Mahalanobis distance classifier did result in the highest accuracy rating and may warrant more investigation in further work.

Image processing techniques were applied to the result of the maximum likelihood classification and compared to each other. Three different approaches were used and evaluated against each other. The sieve and clump operators maintained the highest true positive rate. The results from the decision tree approach reduced the true positive rate, but also had the lowest false positive rate which led to it having the highest accuracy rate.

In the evaluations of both the classification techniques and the image processing methods, the best techniques depend on the application. The maximum likelihood classification and the sieve and clump processing can be thought of as more “liberal”: they classify nearly all positives correctly, but have a high false positive rate. The Mahalanobis distance classifier and the decision tree processing techniques are more

"conservative": they make few false positive classifications, but their true positive rate is low as well. Either set of techniques results in a thematic map that successfully maps roads and trails under canopy.

VII. CONCLUSION

The results of the experiment conducted for this research indicate that roads and trails can be automatically identified under dense tree canopy using LiDAR data. Using classification techniques alone true positive rates of over 83% can be achieved, identifying trails under dense redwood and Douglas fir second growth forests. Applying image processing techniques to this classification product can reduce false positive rates to below 4%, increasing the accuracy of the trail identification to 90.7%. Thematic map products from these processes could prove invaluable for both military and commercial applications. During intelligence preparation of the battlefield (IPB), commanders and intelligence professionals can use this process to define the lines of communications (LOC), which an enemy threat may use to move personnel and supplies through an area of operations.

In the field of LiDAR, there are many ongoing research and development programs in government and commercial sponsored studies. Areas of follow-on research related to this research include:

- Further characterize trails to increase true positive rates and reduce false positive rates.
- Test this process against other data sets with varying terrain and point densities.
- Develop geometric pathway extraction algorithm to produce centerline and trail width vectors.
- Write code to fully automate steps in this process from point cloud to refined trail map output.

The accuracy of road and trail network mapping using LiDAR can be used for quantitative terrain analysis without the need for ground reconnaissance in areas unobservable to electro-optical imagery. LiDAR provides the ability to determine road networks on large scales in denied areas where ground survey is not available. This research demonstrates the value of LiDAR collected data in areas where traditional remote sensing techniques for intelligence preparation of the battlefield are insufficient.

LiDAR holds great potential to provide accurate, detailed, and large coverage area support to ground maneuver forces deployed in diverse and complex environments.

APPENDIX – RANDOM POINT SAMPLING LISTS

ROI name: Random Sample (first_attempt_topo15July /[Green] 201 points)									
ROI rgb value: {0, 255, 0}									
ROI npts: 117									
ID	X	Y	Map X	Map Y	Lat	Lon		Trail = 1	Not Trail = 1
1	1590	1922	6063105.62	1850271.04	37.06384	-122.209		1	
2	1222	1928	6061898.27	1850251.35	37.06373	-122.213		1	
3	1818	1929	6063853.65	1850248.07	37.06382	-122.206			1
4	1556	1930	6062994.07	1850244.79	37.06377	-122.209			1
5	1742	1930	6063604.3	1850244.79	37.0638	-122.207			1
6	1498	1942	6062803.78	1850205.42	37.06365	-122.21			1
7	1206	1945	6061845.78	1850195.58	37.06357	-122.213		1	
8	2171	1947	6065011.78	1850189.02	37.06371	-122.202		1	
9	1474	1950	6062725.04	1850179.17	37.06357	-122.21			1
10	2126	1951	6064864.14	1850175.89	37.06367	-122.203			1
11	1598	1955	6063131.86	1850162.77	37.06355	-122.209		1	
12	1498	1958	6062803.78	1850152.93	37.0635	-122.21			1
13	1582	1964	6063079.37	1850133.24	37.06346	-122.209		1	
14	1464	1980	6062692.23	1850080.75	37.0633	-122.21			1
15	1170	1990	6061727.67	1850047.94	37.06316	-122.213		1	
16	1142	1992	6061635.8	1850041.38	37.06314	-122.214			1
17	1464	1997	6062692.23	1850024.98	37.06315	-122.21			1
18	1528	1998	6062902.2	1850021.69	37.06315	-122.209		1	
19	2265	2007	6065320.18	1849992.17	37.06319	-122.201			1
20	1407	2011	6062505.22	1849979.04	37.06301	-122.211			1
21	1249	2016	6061986.85	1849962.64	37.06294	-122.213			1
22	1057	2023	6061356.93	1849939.67	37.06285	-122.215		1	
23	1701	2044	6063469.79	1849870.78	37.06276	-122.207			1
24	1096	2049	6061484.88	1849854.37	37.06262	-122.214			1
25	1678	2062	6063394.33	1849811.72	37.0626	-122.208			1
26	1759	2075	6063660.08	1849769.07	37.06249	-122.207			1
27	1611	2081	6063174.51	1849749.39	37.06241	-122.208			1
28	1615	2082	6063187.64	1849746.1	37.06241	-122.208			1
29	2213	2089	6065149.57	1849723.14	37.06244	-122.202			1
30	1073	2091	6061409.42	1849716.58	37.06224	-122.215			1
31	1101	2092	6061501.29	1849713.3	37.06223	-122.214			1
32	1041	2102	6061304.44	1849680.49	37.06213	-122.215			1
33	1076	2104	6061419.27	1849673.93	37.06212	-122.214			1
34	1094	2106	6061478.32	1849667.36	37.0621	-122.214			1
35	1066	2123	6061386.46	1849611.59	37.06195	-122.215			1
36	1242	2123	6061963.89	1849611.59	37.06198	-122.213			1
37	1550	2127	6062974.38	1849598.47	37.06199	-122.209			1
38	1958	2134	6064312.96	1849575.5	37.06199	-122.205		1	
39	985	2147	6061120.71	1849532.85	37.06172	-122.215		1	
40	1296	2177	6062141.05	1849434.43	37.0615	-122.212			1
41	1234	2178	6061937.64	1849431.14	37.06148	-122.213			1
42	1335	2179	6062269	1849427.86	37.06149	-122.212			1
43	1285	2179	6062104.96	1849427.86	37.06148	-122.212			1
44	1111	2179	6061534.1	1849427.86	37.06145	-122.214			1
45	1130	2189	6061596.43	1849395.06	37.06136	-122.214			1
46	1642	2213	6063276.22	1849316.32	37.06123	-122.208			1

47	1054	2217	6061347.09	1849303.19	37.0611	-122.215		1	
48	2331	2223	6065536.71	1849283.51	37.06125	-122.2		1	
49	1535	2228	6062925.17	1849267.1	37.06108	-122.209			1
50	1146	2233	6061648.93	1849250.7	37.06097	-122.214		1	
51	1555	2239	6062990.79	1849231.01	37.06098	-122.209			1
52	1573	2253	6063049.84	1849185.08	37.06086	-122.209			1
53	998	2262	6061163.36	1849155.55	37.06068	-122.215		1	
54	2299	2273	6065431.73	1849119.47	37.0608	-122.201		1	
55	976	2286	6061091.18	1849076.81	37.06046	-122.216		1	
56	1076	2287	6061419.27	1849073.53	37.06047	-122.214			1
57	1647	2296	6063292.62	1849044.01	37.06048	-122.208			1
58	1865	2297	6064007.84	1849040.73	37.06051	-122.206		1	
59	1638	2304	6063263.1	1849017.76	37.06041	-122.208			1
60	1648	2325	6063295.9	1848948.86	37.06022	-122.208			1
61	2094	2330	6064759.16	1848932.46	37.06025	-122.203			1
62	1645	2332	6063286.06	1848925.9	37.06016	-122.208			1
63	1177	2336	6061750.63	1848912.77	37.06005	-122.213			1
64	1509	2356	6062839.87	1848847.16	37.05992	-122.21			1
65	1428	2394	6062574.12	1848722.48	37.05956	-122.21			1
66	1012	2435	6061209.29	1848587.97	37.05913	-122.215		1	
67	1125	2439	6061580.03	1848574.85	37.05911	-122.214		1	
68	1705	2457	6063482.91	1848515.79	37.05904	-122.207		1	
69	1333	2493	6062262.44	1848397.68	37.05866	-122.212		1	
70	1362	2494	6062357.59	1848394.4	37.05865	-122.211		1	
71	1037	2532	6061291.31	1848269.73	37.05826	-122.215			1
72	1719	2549	6063528.84	1848213.96	37.05822	-122.207		1	
73	1709	2564	6063496.03	1848164.74	37.05808	-122.207		1	
74	2362	2574	6065638.42	1848131.93	37.0581	-122.2		1	
75	1213	2584	6061868.74	1848099.13	37.05782	-122.213			1
76	1005	2592	6061186.33	1848072.88	37.05771	-122.215		1	
77	1660	2600	6063335.27	1848046.63	37.05775	-122.208		1	
78	2255	2619	6065287.37	1847984.3	37.05767	-122.201			1
79	1283	2627	6062098.4	1847958.05	37.05744	-122.212		1	
80	1405	2651	6062498.66	1847879.31	37.05725	-122.211			1
81	1635	2662	6063253.25	1847843.22	37.05718	-122.208			1
82	2080	2684	6064713.22	1847771.04	37.05706	-122.203			1
83	1203	2684	6061835.93	1847771.04	37.05692	-122.213			1
84	1159	2685	6061691.58	1847767.76	37.0569	-122.213		1	
85	1345	2694	6062301.81	1847738.23	37.05685	-122.211			1
86	1238	2709	6061950.76	1847689.02	37.0567	-122.213		1	
87	1212	2718	6061865.46	1847659.49	37.05661	-122.213		1	
88	1067	2732	6061389.74	1847613.56	37.05646	-122.214		1	
89	1065	2750	6061383.18	1847554.51	37.0563	-122.214		1	
90	2331	2756	6065536.71	1847534.82	37.05645	-122.2		1	
91	1705	2759	6063482.91	1847524.98	37.05632	-122.207		1	
92	2322	2768	6065507.19	1847495.45	37.05634	-122.2		1	
93	1692	2788	6063440.26	1847429.84	37.05606	-122.207		1	
94	1533	2788	6062918.61	1847429.84	37.05603	-122.209		1	
95	1581	2793	6063076.09	1847413.43	37.056	-122.209			1
96	1109	2794	6061527.53	1847410.15	37.05591	-122.214		1	
97	1067	2795	6061389.74	1847406.87	37.05589	-122.214			1

98	1536	2795	6062928.45	1847406.87	37.05597	-122.209		1	
99	1601	2809	6063141.7	1847360.94	37.05585	-122.208		1	
100	1221	2809	6061894.99	1847360.94	37.05579	-122.213			1
101	2096	2814	6064765.72	1847344.53	37.05589	-122.203		1	
102	997	2817	6061160.08	1847334.69	37.05568	-122.215		1	
103	2064	2817	6064660.73	1847334.69	37.05586	-122.203			1
104	2145	2818	6064926.48	1847331.41	37.05586	-122.202		1	
105	1707	2820	6063489.47	1847324.85	37.05577	-122.207		1	
106	1031	2831	6061271.63	1847288.76	37.05556	-122.215			1
107	1436	2842	6062600.37	1847252.67	37.05553	-122.21		1	
108	1178	2844	6061753.91	1847246.11	37.05547	-122.213		1	
109	2179	2851	6065038.03	1847223.14	37.05557	-122.202			1
110	1684	2855	6063414.01	1847210.02	37.05545	-122.207		1	
111	1752	2857	6063637.11	1847203.46	37.05545	-122.207		1	
112	1022	2857	6061242.1	1847203.46	37.05533	-122.215			1
113	1260	2870	6062022.94	1847160.81	37.05525	-122.212		1	
114	2254	2870	6065284.09	1847160.81	37.05541	-122.201			1
115	1984	2872	6064398.26	1847154.25	37.05535	-122.204		1	
116	2107	2875	6064801.81	1847144.4	37.05534	-122.203			1
117	1638	2879	6063263.1	1847131.28	37.05523	-122.208			1

ROI name: Random Sample (first_attempt_topo15July /[Red] 1228 points)									
ROI rgb value: {255, 0, 0}									
ROI npts: 46									

ID	X	Y	Map X	Map Y	Lat	Lon		Trail = 1	Not Trail = 1
1	1066	1791	6061386.5	1850700.8	37.06494	-122.2147			1
2	1060	1809	6061366.8	1850641.8	37.06477	-122.2147			1
3	1384	1815	6062429.8	1850622.1	37.06477	-122.2111			1
4	1066	1832	6061386.5	1850566.3	37.06457	-122.2146			1
5	1391	1835	6062452.7	1850556.5	37.06459	-122.211			1
6	1222	1843	6061898.3	1850530.2	37.06449	-122.2129			1
7	2343	1850	6065576.1	1850507.3	37.06462	-122.2003			1
8	1464	1852	6062692.2	1850500.7	37.06445	-122.2102			1
9	1161	1856	6061698.1	1850487.6	37.06437	-122.2136			1
10	2271	1884	6065339.9	1850395.7	37.0643	-122.2011			1
11	1304	1892	6062167.3	1850369.5	37.06407	-122.212			1
12	986	1904	6061124	1850330.1	37.06391	-122.2155			1
13	2327	1918	6065523.6	1850284.2	37.064	-122.2005			1
14	2346	1922	6065585.9	1850271	37.06397	-122.2002			1
15	1447	1956	6062636.5	1850159.5	37.06351	-122.2103			1
16	1742	1987	6063604.3	1850057.8	37.06328	-122.207			1
17	1657	2026	6063325.4	1849929.8	37.06292	-122.208			1
18	1294	2091	6062134.5	1849716.6	37.06227	-122.212			1
19	2178	2128	6065034.8	1849595.2	37.06208	-122.2021		1	
20	1233	2151	6061934.4	1849519.7	37.06172	-122.2127			1
21	1546	2217	6062961.3	1849303.2	37.06118	-122.2092			1
22	1244	2270	6061970.5	1849129.3	37.06065	-122.2126			1
23	1299	2284	6062150.9	1849083.4	37.06053	-122.2119			1
24	2188	2285	6065067.6	1849080.1	37.06067	-122.2019			1
25	1608	2325	6063164.7	1848948.9	37.06022	-122.2085			1
26	1968	2327	6064345.8	1848942.3	37.06026	-122.2044			1
27	1078	2331	6061425.8	1848929.2	37.06007	-122.2144			1
28	2049	2357	6064611.5	1848843.9	37.06	-122.2035			1
29	1545	2361	6062958	1848830.8	37.05988	-122.2092			1
30	1560	2365	6063007.2	1848817.6	37.05985	-122.209			1
31	1937	2380	6064244.1	1848768.4	37.05977	-122.2047			1
32	1048	2418	6061327.4	1848643.7	37.05929	-122.2147			1
33	2296	2436	6065421.9	1848584.7	37.05933	-122.2007			1
34	1996	2446	6064437.6	1848551.9	37.05919	-122.2041			1
35	1742	2450	6063604.3	1848538.8	37.05911	-122.2069			1
36	2101	2462	6064782.1	1848499.4	37.05906	-122.2029			1
37	1548	2468	6062967.8	1848479.7	37.05892	-122.2091		1	
38	2063	2515	6064657.5	1848325.5	37.05858	-122.2033			1
39	1248	2537	6061983.6	1848253.3	37.05825	-122.2125			1
40	2013	2539	6064493.4	1848246.8	37.05835	-122.2039			1
41	2324	2616	6065513.8	1847994.1	37.05771	-122.2003			1
42	1543	2688	6062951.4	1847757.9	37.05694	-122.2091			1
43	1651	2762	6063305.8	1847515.1	37.05629	-122.2079			1
44	1080	2774	6061432.4	1847475.8	37.05608	-122.2143		1	
45	1902	2816	6064129.2	1847338	37.05584	-122.205			1
46	1161	2891	6061698.1	1847091.9	37.05504	-122.2134			1

ROI name: Random Sample (first_attempt_topo15July /[Blue] 585 points)									
ROI rgb value: (0, 0, 255)									
ROI npts: 65									
ID	X	Y	Map X	Map Y	Lat	Lon		Trail = 1	Not Trail = 1
1	1660	1721	6063335.3	1850930.5	37.06567	-122.208			1
2	2274	1748	6065349.7	1850841.9	37.06552	-122.2011			1
3	1463	1757	6062689	1850812.4	37.06531	-122.2102			1
4	1647	1825	6063292.6	1850589.3	37.06473	-122.2081			1
5	2321	1843	6065503.9	1850530.2	37.06468	-122.2005			1
6	1464	1875	6062692.2	1850425.2	37.06425	-122.2102			1
7	1448	1885	6062639.7	1850392.4	37.06415	-122.2103			1
8	1770	1891	6063696.2	1850372.7	37.06415	-122.2067			1
9	1163	1910	6061704.7	1850310.4	37.06388	-122.2135			1
10	1386	1943	6062436.3	1850202.1	37.06362	-122.211			1
11	2344	2034	6065579.4	1849903.6	37.06296	-122.2002			1
12	2251	2052	6065274.3	1849844.5	37.06278	-122.2013			1
13	2069	2076	6064677.1	1849765.8	37.06254	-122.2033			1
14	1960	2092	6064319.5	1849713.3	37.06237	-122.2045			1
15	2052	2096	6064621.4	1849700.2	37.06235	-122.2035			1
16	2157	2105	6064965.9	1849670.7	37.06229	-122.2023			1
17	1168	2131	6061721.1	1849585.3	37.06189	-122.2134			1
18	2199	2133	6065103.6	1849578.8	37.06204	-122.2018			1
19	1155	2141	6061678.5	1849552.5	37.0618	-122.2136			1
20	2242	2165	6065244.7	1849473.8	37.06176	-122.2014			1
21	1953	2226	6064296.6	1849273.7	37.06116	-122.2046			1
22	1391	2227	6062452.7	1849270.4	37.06106	-122.2109			1
23	1956	2293	6064306.4	1849053.9	37.06056	-122.2045			1
24	1164	2301	6061708	1849027.6	37.06036	-122.2134			1
25	1166	2306	6061714.5	1849011.2	37.06031	-122.2134			1
26	1142	2328	6061635.8	1848939	37.06011	-122.2137			1
27	2058	2332	6064641.1	1848925.9	37.06023	-122.2034			1
28	1991	2341	6064421.2	1848896.4	37.06013	-122.2041			1
29	1988	2344	6064411.4	1848886.5	37.06011	-122.2042			1
30	1365	2403	6062367.4	1848693	37.05947	-122.2112			1
31	2329	2411	6065530.2	1848666.7	37.05956	-122.2003			1
32	1111	2418	6061534.1	1848643.7	37.0593	-122.214			1
33	1080	2442	6061432.4	1848565	37.05908	-122.2144			1
34	968	2489	6061064.9	1848410.8	37.05863	-122.2156			1
35	1494	2494	6062790.7	1848394.4	37.05867	-122.2097			1
36	1903	2569	6064132.5	1848148.3	37.05807	-122.2051			1
37	1521	2582	6062879.2	1848105.7	37.05789	-122.2094			1
38	2221	2592	6065175.8	1848072.9	37.05791	-122.2015			1
39	1521	2598	6062879.2	1848053.2	37.05774	-122.2094			1
40	1483	2600	6062754.6	1848046.6	37.05772	-122.2098			1
41	1451	2608	6062649.6	1848020.4	37.05764	-122.2102			1
42	1886	2626	6064076.7	1847961.3	37.05755	-122.2053			1
43	1533	2626	6062918.6	1847961.3	37.05749	-122.2092			1
44	1479	2634	6062741.4	1847935.1	37.05741	-122.2098			1
45	1548	2646	6062967.8	1847895.7	37.05731	-122.2091			1
46	2164	2652	6064988.8	1847876	37.05736	-122.2021			1
47	2255	2660	6065287.4	1847849.8	37.0573	-122.2011			1
48	1972	2669	6064358.9	1847820.3	37.05718	-122.2043			1

49	1275	2674	6062072.2	1847803.9	37.05702	-122.2121			1
50	1123	2686	6061573.5	1847764.5	37.05688	-122.2138			1
51	2303	2690	6065444.9	1847751.4	37.05704	-122.2006			1
52	1641	2699	6063272.9	1847721.8	37.05685	-122.208			1
53	1494	2702	6062790.7	1847712	37.0568	-122.2097			1
54	1897	2716	6064112.8	1847666.1	37.05674	-122.2051			1
55	1686	2725	6063420.6	1847636.5	37.05663	-122.2075		1	
56	1171	2726	6061731	1847633.3	37.05653	-122.2133			1
57	2285	2750	6065385.8	1847554.5	37.0565	-122.2008			1
58	1021	2769	6061238.8	1847492.2	37.05612	-122.215			1
59	1855	2783	6063975	1847446.2	37.05613	-122.2056			1
60	1466	2808	6062698.8	1847364.2	37.05584	-122.2099		1	
61	1287	2811	6062111.5	1847354.4	37.05578	-122.212			1
62	1199	2838	6061822.8	1847265.8	37.05553	-122.2129			1
63	1093	2840	6061475	1847259.2	37.05549	-122.2141		1	
64	1119	2852	6061560.3	1847219.9	37.05539	-122.2138			1
65	1080	2892	6061432.4	1847088.6	37.05502	-122.2143			1

ROI name: Random Sample (first_attempt_topo15July /[Yellow] 2616 points)									
ROI rgb value: (255, 255, 0)									
ROI npts: 39									
ID	X	Y	Map X	Map Y	Lat	Lon		Trail = 1	Not Trail = 1
1	1274	1744	6062068.9	1850855	37.0654	-122.2123			1
2	2321	1747	6065503.9	1850845.2	37.06554	-122.2006			1
3	1864	1753	6064004.6	1850825.5	37.06541	-122.2057			1
4	1527	1767	6062898.9	1850779.6	37.06523	-122.2095			1
5	1851	1794	6063961.9	1850691	37.06504	-122.2058			1
6	1902	1965	6064129.2	1850130	37.06351	-122.2052			1
7	1962	1977	6064326.1	1850090.6	37.06341	-122.2045			1
8	1969	1979	6064349.1	1850084	37.06339	-122.2045			1
9	1877	2017	6064047.2	1849959.4	37.06304	-122.2055			1
10	2168	2047	6065001.9	1849860.9	37.06281	-122.2022			1
11	2193	2078	6065084	1849759.2	37.06254	-122.2019			1
12	1864	2104	6064004.6	1849673.9	37.06225	-122.2056			1
13	1875	2108	6064040.7	1849660.8	37.06221	-122.2055			1
14	1133	2125	6061606.3	1849605	37.06194	-122.2138			1
15	2280	2138	6065369.4	1849562.4	37.06201	-122.2009			1
16	2349	2173	6065595.8	1849447.6	37.06171	-122.2002		1	
17	1497	2187	6062800.5	1849401.6	37.06144	-122.2097			1
18	1528	2193	6062902.2	1849381.9	37.06139	-122.2094			1
19	1874	2290	6064037.4	1849063.7	37.06058	-122.2055		1	
20	1452	2326	6062652.9	1848945.6	37.06018	-122.2102			1
21	1213	2403	6061868.7	1848693	37.05945	-122.2129			1
22	1662	2434	6063341.8	1848591.3	37.05924	-122.2078			1
23	1704	2470	6063479.6	1848473.1	37.05893	-122.2073			1
24	1678	2481	6063394.3	1848437.1	37.05882	-122.2076			1
25	1098	2525	6061491.5	1848292.7	37.05833	-122.2141			1
26	1367	2530	6062374	1848276.3	37.05833	-122.2111			1
27	1794	2533	6063774.9	1848266.5	37.05837	-122.2063			1
28	1637	2537	6063259.8	1848253.3	37.05831	-122.2081		1	
29	2266	2548	6065323.5	1848217.2	37.05832	-122.201			1
30	1244	2548	6061970.5	1848217.2	37.05815	-122.2125			1
31	1295	2553	6062137.8	1848200.8	37.05811	-122.2119			1
32	1161	2560	6061698.1	1848177.9	37.05803	-122.2134			1
33	1716	2617	6063519	1847990.9	37.0576	-122.2072			1
34	1008	2644	6061196.2	1847902.3	37.05724	-122.2151			1
35	2056	2740	6064634.5	1847587.3	37.05655	-122.2033			1
36	2370	2768	6065664.7	1847495.5	37.05635	-122.1998			1
37	1022	2796	6061242.1	1847403.6	37.05588	-122.2149			1
38	1179	2801	6061757.2	1847387.2	37.05586	-122.2132			1
39	1178	2801	6061753.9	1847387.2	37.05586	-122.2132			1

THIS PAGE INTENTIONALLY LEFT BLANK

LIST OF REFERENCES

About Us - Swanton Pacific Ranch - Cal Poly Retrieved 8/16/2011, from http://www.spranch.org/about.ldml

Abshire, J. B., Sun, X., Riris, H., Sirota, J. M., McGarry, J. F., Palm, S., Liiva, P. (2005). Geoscience laser altimeter system (GLAS) on the ICESat Mission: on-orbit measurement performance. *Geophysical Research Letters, 32*(21), L21S02. doi:10.1029/2005GL024028

Baltsavias, E. P. (1999). Airborne laser scanning: basic relations and formulas. *ISPRS Journal of Photogrammetry and Remote Sensing, 54*(2–3), 199–214. doi: 10.1016/S0924–2716(99)00015–5

Carabajal, C. C., Harding, D. J., Luthcke, S. B., Fong, W., Rowton, S. C., & Frawley, J. J. (1999). Processing of shuttle laser altimeter range and return pulse data in support of SLA-02. *International Archives of Photogrammetry and Remote Sensing, 32*(3), 64–72.

Clode, S., Rottensteiner, F., Kootsookos, P., & Zelniker, E. (2007). Detection and vectorization of roads from lidar data. *Photogrammetric Engineering and Remote Sensing, 73*(5), 517–535.

Crutchley, S., & Crow, P. (2009). *The light fantastic: Using airborne laser scanning in archeological survey*. Swindon: English Heritage.

David, N., Mallet, C., Pons, T., Chauve, A., & Bretar, F. (2009). Pathway detection and geometrical description from ALS data in forested mountaneous area. Paris, France. *, IAPRS Vol. XXXVIII*(Part 3/W8) 242–247.

De Veaux, R. D., Velleman, P. F., & Bock, D. E. (2009). *Intro stats* (3rd ed.). Boston; London: Pearson/Addison-Wesley.

Diaz, J. C. F. (2011, Lifting the canopy veil: airborne LiDAR for archeology of forested areas. *Imaging Notes Magazine, 26* Retrieved 8/11/2011 from http://www.imagingnotes.com/go/article_freeJ.php?mp_id=264#1

Espinoza, F., & Owens, R. E. (2007). *Identifying roads and trails hidden under canopy using Lidar.* (M.S. thesis, Naval Postgraduate School), Monterey, CA.

ESRI. *Esri Products:A Complete GIS and Mapping Software System* Retrieved 8/19/2011, from http://www.esri.com/products/index.html#desktop_gis_panel

ESRI. (2010). *ArcMap (Version 10.0)*. Redlands, CA: Economic and Social Research Institute (ESRI).

Fawcett, T. (2004). *ROC Graphs: Notes and Practical Considerations for Researchers.* Palo Alto, CA: HP Laboratories.

Food and Agriculture Organization of the United Nations. (2010). *Global forest resources assessment 2010: main report*. Rome: Food and Agriculture Organization of the United Nations. Retrieved from http://www.fao.org/docrep/013/i1757e/i1757e.pdf

Franken, P. A. M., & Flos, S. J. (2005). Using a helicopter based laser altimetry system (FLI-MAP) to carry out effective dike maintenance and construction policy. *Floods, from Defence to Management,* 145–151.

Google. *Turning Photos into Street View – Google Maps with Street View* Retrieved 8/11/2011, from http://www.google.com/intl/en_ALL/help/maps/streetview/technology/photos-into-street-view.html

Gordon, P., & Charles, T. (2008). Airborne and spaceborne laser profilers and scanners. *Topographic laser ranging and scanning.* CRC Press. doi:10.1201/9781420051438

Harding, D. (2001). *SLA-1 Standard Data Product Version 2 (SDP v2)* Retrieved 8/11/2011, from http://denali.gsfc.nasa.gov/sla/sla/srowton/

Heritage, G. L., & Large, A. R. G. (2009). *Laser scanning for the environmental sciences*. Chichester, UK; Hoboken, NJ: Wiley-Blackwell.

ITT Visual Information Solutions. (2010). *ENVI Help*. Boulder, Colorado: ITT Visual Information Solutions.

Lefsky, M. (2010). *NASA - First-of-its-Kind Map Depicts Global Forest Heights* Retrieved 8/11/2011, from http://www.nasa.gov/topics/earth/features/forest-height-map.html

NASA. (1994). *NASA - Lidar In-space Technology Experiment (LITE)* Retrieved 8/11/2011, from http://www.nasa.gov/centers/langley/news/factsheets/LITE.html

Optech. (2011). *Optech ALTM Airborne Laser Terrain Mapper.* Retrieved 8/02/2011, from http://www.optech.ca/prodaltm.htm

Richards, J. A., & Jia, X. (2006). *Remote Sensing Digital Image Analysis: An Introduction* (4th ed.). Berlin: Springer.

Richmond, R. D., & Cain, S. C. (2010). *Direct-detection LADAR systems*. Bellingham, Wash: SPIE Press.

Schutz, B. E., Zwally, H. J., Shuman, C. A., Hancock, D., & DiMarzio, J. P. (2005). Overview of the ICESat Mission. *Geophysical Research Letters, 32*(21), L21S01. doi:10.1029/2005GL024009

Shan, J., & Toth, C. K. (2009). *Topographic laser ranging and scanning: Principles and processing*. Boca Raton: CRC Press/Taylor & Francis Group.

Sibson, R. (1981). A Brief Description of Natural Neighbor Interpolation. *Interpolating Multivariate Data* (pp. 21–36). New York: John Wiley & Sons.

Szeliski, R. (2011). *Computer vision: Algorithms and applications*. New York: Springer.

Vosselman, G., & Maas, H. (Eds.). (2010). *Airborne and terrestrial laser scanning*. Boca Raton, Florida: CRC Press LLC.

White, R. A. (2010). *Accuracy of Forest Road and Stream Channel Characteristics Derived from LiDAR in Forested Mountain Conditions.* (M.S. thesis, California Polytechnic State University) San Luis Obispo, CA.

White, R. A., Dietterick, B. C., Mastin, T., & Strohman, R. (2010). Forest Roads Mapped Using LiDAR in Steep Forested Terrain. *Remote Sensing, 2*(4), 1120–1141. doi:10.3390/rs2041120

THIS PAGE INTENTIONALLY LEFT BLANK

INITIAL DISTRIBUTION LIST

1. Defense Technical Information Center
   Ft. Belvoir, Virginia

2. Dudley Knox Library
   Naval Postgraduate School
   Monterey, California

3. Richard C. Olsen
   Naval Postgraduate School
   Monterey, California

4. Kristen Tsolis
   Naval Postgraduate School
   Monterey, California

5. Dan C. Boger
   Naval Postgraduate School
   Monterey, California

6. Rudy Panholzer
   Naval Postgraduate School
   Monterey, California